AzTEC 1.1-mm images of 16 radio galaxies at 0.5 < *z* < 5.2 and a quasar at *z* = 6.3

A. Humphrey,[1]⋆ M. Zeballos,[1] I. Aretxaga,[1] D. H. Hughes,[1] M. S. Yun,[2] R. Cybulski,[2] Grant W. Wilson,[2] J. Austermann,[3] H. Ezawa,[4] R. Kawabe,[4] K. Kohno,[5,6] T. Perera,[7] K. Scott,[2,8] D. Sánchez-Arguelles[1] and R. Gutermuth[9]

[1]*Instituto Nacional de Astrofísica, Óptica y Electrónica (INAOE), Aptdo. Postal 51 y 216, 72000 Puebla, Pue., Mexico*
[2]*Department of Astronomy, University of Massachusetts, Amherst, MA 01003, USA*
[3]*Center for Astrophysics and Space Astronomy, University of Colorado, Boulder, CO 80309, USA*
[4]*Nobeyama Radio Observatory, National Astronomical Observatory of Japan, Minamimaki, Minamisaku, Nagano 384-1305, Japan*
[5]*Institute of Astronomy, University of Tokyo, 2-21-1 Osawa, Mitaka, Tokyo 181-0015, Japan*
[6]*Research Center for the Early Universe, University of Tokyo, 7-3-1 Hongo, Bunkyo, Tokyo 113-0033, Japan*
[7]*Department of Physics, Illinois Wesleyan University, Bloomington, IL 61701, USA*
[8]*Department of Physics and Astronomy, University of Pennsylvania, Philadelphia, PA 19104, USA*
[9]*Smith College, Northampton, MA 01063, USA*

ABSTRACT

We present 1.1-mm observations for a sample of 16 powerful radio galaxies at 0.5 < *z* < 5.2 and a radio-quiet quasar at *z* = 6.3, obtained using the AzTEC bolometer array mounted on the Atacama Submillimetre Telescope Experiment (ASTE) or the James Clerk Maxwell Telescope (JCMT). This paper more than doubles the number of high-*z* radio galaxies imaged at millimetre/submillimetre wavelengths. We detect probable millimetre-wave counterparts for 11 of the active galaxies. The six active galaxies that do not have a probable millimetre counterpart in our images nevertheless have one or more likely associated millimetric source. Thus, we conclude that powerful (radio-loud) active galaxies at high-*z* are beacons for finding luminous millimetre/submillimetre galaxies at high-*z*. The flux densities of our AzTEC *counterparts* imply star formation rates ranging from <200 to ∼1300 M⊙ yr^{-1}. In addition, we find that for the radio galaxies the 1.1-mm flux density is anticorrelated with the largest angular size of the radio source.

We also present new *Spitzer* imaging observations of several active galaxies in our sample. Combining these with archival data, we examine the mid-infrared colours of our sample. We find that radio galaxies for which we have detected a probable 1.1-mm counterpart have mid-infrared colours consistent with dusty starbursts, and are usually bluer than high-*z Spitzer*-selected active galaxies. In addition, we find arcs of 24-µm sources extending across ∼200–500 kpc, apparently associated with three of the radio galaxies.

Key words: galaxies: active – galaxies: high-redshift – quasars: general – galaxies: starburst – cosmology: observations.

1 INTRODUCTION

Powerful, high-*z* radio galaxies (*z* ≥ 0.5: HzRGs) continue to play a key role in cosmological investigations. Their high luminosities at radio and optical wavelengths make them useful as beacons for finding massive elliptical galaxies and their progenitors out to high redshifts (e.g. Dunlop et al. 1996; Röttgering et al. 1997; McLure et al. 1999), and provide unique opportunities to study their host galaxy and environment (e.g. Venemans et al. 2007).

Many HzRGs are embedded within haloes of ionized gas which are extended on spatial scales of tens of kpc, and which emit luminous emission lines from various species (e.g. McCarthy, Spinrad & van Breugel 1995; Reuland et al. 2003a; Villar-Martín et al. 2003). Spatially resolved kinematic studies of these haloes suggest that the cold gas comprising many of these haloes is in infall towards the centre of the host galaxy (Humphrey et al. 2007), while in others it is being strongly disturbed by the radio jets (e.g. Best, Röttgering & Longair 2000; Nesvadba et al. 2006). In most cases, ratios between

⋆E-mail: ajh@inaoep.mx

emission lines imply that the radiation field of the active galactic nucleus (AGN) is the dominant ionization mechanism for the haloes, although shocks may make a fractional contribution in some cases (e.g. Vernet et al. 2001; Humphrey et al. 2008). Modelling of the flux ratio Lyα/He IIλ1640 determined for one-dimensional spectra has revealed an excess of Lyα emission above the predictions of AGN photoionization models (Villar-Martín et al. 2007), which suggests the presence of star-forming regions in the giant gaseous haloes (see also Hatch et al. 2009).

Millimetre emission provides an alternative means by which the star formation history of HzRGs can be probed. Several tens of HzRGs have now been detected at millimetre wavelengths, with the detection rate rising from $\sim$15 per cent at $z < 2.5$ to $\gtrsim$75 per cent at $z > 2.5$ (Archibald et al. 2001; Reuland et al. 2004). Millimetric observations are sensitive to cold dust that is re-radiating emission received from young stars: implied rates of star formation range from a few hundred to $\sim$1500 M$_\odot$ yr^{-1} (Dunlop et al. 1994; Archibald et al. 2001; Reuland et al. 2004). These millimetre/submillimetre detected radio galaxies are not typical of the wider population of millimetre/submillimetre selected galaxies (MMGs hereafter): unlike the vast majority of MMGs, the millimetre emission from radio galaxies is often extended on spatial scales of $\gtrsim$100 kpc (e.g. Stevens et al. 2003) can show morphological complexity (Greve et al. 2007) and is not always spatially coincident with the radio-optical nucleus of the AGN and host galaxy (Ivison et al. 2008). Several HzRGs also appear to have MMGs as companions, or are associated with an overdensity of MMGs (Ivison et al. 2000; Stevens et al. 2003; see also Priddey, Ivison & Isaak 2008; Stevens et al. 2010).

In this paper we present images and measure 1.1-mm flux densities for a sample of 16 powerful radio galaxies at $0.5 < z < 5.2$ and a radio-quiet quasar at $z = 6.3$, observed with the AzTEC bolometer array instrument (Wilson et al. 2008) mounted on the Atacama Submillimetre Telescope Experiment (ASTE, Ezawa et al. 2004) or the James Clerk Maxwell Telescope (JCMT), as a part of the AzTEC/ASTE Cluster Environment Survey (ACES, Zeballos et al., in preparation). Throughout this paper we adopt a flat Universe with $H_0 = 71$ km s^{-1} Mpc^{-1}, $\Omega_M = 0.27$ and $\Omega_\Lambda = 0.73$. In this cosmology 1 arcsec corresponds to 5.7–8.6 kpc for $0.5 < z < 6.3$.

2 DATA

2.1 Sample

For this investigation we have selected 16 powerful radio galaxies at $0.5 < z < 5.2$ from compendia of high-z radio galaxies (e.g. Miley & De Breuck 2008). This sample is designed to cover a large range of z so as to allow investigations into the possible cosmic evolution of the properties of powerful radio galaxies and their environments. The lower limit to z was set at 0.5 in order to minimize the possible contribution to the observer-frame 1.1-mm emission from the Sunyaev–Zel'dovich effect (SZE), though it is not impossible that the SZE still makes a significant (i.e., a few mJy) contribution to the 1.1-mm flux densities of radio galaxies at $0.5 < z \lesssim 1$ (e.g. High et al. 2010; Menanteau et al. 2010; Foley et al. 2011). However, one of our galaxies in that redshift range (MRC 2008$-$068: $z = 0.55$) has been imaged in X-rays (*XMM–Newton* observation ID 0502510501), but it shows no evidence for the extended X-ray emitting gas needed to produce a significant SZE signal. Since we have no evidence for any SZE signal in the $0.5 < z \lesssim 1$ radio galaxies, we are unable to make a realistic correction for a possible SZE contamination.

Our sample also covers a substantial range in the (projected) size of the radio source, with diameters ranging between 0.2 and 390 kpc, in order to study the possible relationship between the growth or containment of the radio source and the millimetric properties of the galaxy. We purposefully put into the sample some radio galaxies that are known to reside in clusters or protoclusters (e.g. PKS 1138$-$262: Pentericci et al. 1997), some radio galaxies that do not appear to reside in overdense environments (e.g. MRC 2048$-$272: Venemans et al. 2007), as well as radio galaxies for which cluster/overdensity analyses have yet to be undertaken.

In the process of selecting our sample, no strong preference was given to any other observational properties of the galaxies, but several strong biases necessarily exist due to processes involved in the initial identification of the radio galaxies. First, the galaxies are all near the top of the radio luminosity function for radio galaxies, and the majority of them were selected from radio catalogues on the basis of their ultrasteep radio spectra ($S_\nu \propto \nu^\alpha$ where $\alpha \lesssim -1$: e.g. Chambers et al. 1996). In addition, these galaxies all have luminous UV–optical continuum emission, as required for the identification of the optical counterpart. They also all emit luminous UV–optical emission lines from spatially extended regions of cold gas, photoionized by the active nucleus: such conditions are necessary for obtaining a spectroscopic redshift. In summary, our sample is a subset of high-z radio galaxies which have very powerful, steep-spectrum radio sources, together with luminous UV–optical continuum and line emission.

It is important to note that roughly 30 per cent of high-z radio galaxy candidates do not show bright optical/UV emission lines (e.g. Miley & De Breuck 2008), meaning that samples selected in the above way may not be completely representative of high-z radio galaxies. Interestingly, it has been suggested that these 'no-line' radio galaxies are very dusty, based on millimetre/submillimetre detections thereof (Reuland et al. 2003b; Reuland 2005).

Our sample also includes the $z = 6.28$ radio-quiet quasar Sloan Digital Sky Survey (SDSS) J103027.10+052455.0 (Fan et al. 2001). Throughout this paper, we abbreviate this source name to J1030+0524. When the observations were being prepared, this source held the record for the active galaxy with the highest known z. It is currently unclear whether this quasar resides in a rich environment (Stiavelli et al. 2005; Willott et al. 2005; Priddey et al. 2008; Kim et al. 2009).

2.2 AzTEC 1.1-mm observations

In the pilot of this programme, the field of 4C+41.17 was mapped utilizing unchopped raster scans, using the AzTEC bolometer array (Wilson et al. 2008) with the James Clerk Maxwell Telescope (JCMT) during 2005 December. The rest of our sample was observed during 2007 May to October or 2008 July to December, with AzTEC at the Atacama Submillimetre Telescope Experiment (ASTE), using a Lissajous pattern centred on the targeted active galaxy. The observations were made under excellent weather conditions, with effective atmospheric opacities for each field falling within the range $0.03 \leq \tau \leq 0.06$. Integration times varied between 16 and 35 h per field. The resulting maps cover areas ranging from 170 to 300 arcmin^2 for a 50 per cent coverage cut.

The data reduction procedure is given in Scott et al. (2008) with modifications discussed by Scott et al. (2010) and Downes et al. (2011). The basic steps are (i) to clean the raw time-stream data of spikes due to cosmic rays and instrumental glitches; (ii) to then clean using principal component analysis; (iii) to calibrate and bin the bolometer signals to produce a map for each individual observation,

with a pixel size of $2 \times 2 \, \text{arcsec}^2$ for 4C+41.17 or $3 \times 3 \, \text{arcsec}^2$ for the rest of the sample; and (iv) to co-add maps and apply a Wiener filter. The observations, the data reduction and the source detection/extraction are described in greater detail by Zeballos et al. (in preparation).

2.3 *Spitzer* imaging

The *Spitzer* (Werner et al. 2004) observations of the active galaxies come from both archival data and observations from PID 50610 (PI: M. S. Yun). 15 of the galaxies were observed with the Multiband Imaging Photometer for Spitzer (MIPS: Rieke et al. 2004) at 24 μm, and 14 were observed with the Infrared Array Camera (IRAC: Fazio et al. 2004) at 3.6, 4.5, 5.8 and 8.0 μm. Our new observations (PID 50610) consist of five MIPS maps (MRC 2201−555; MRC 2008−068; MRC 0355−037; TN J2009−3040; TN J1338−1942) and three IRAC maps (MRC 2201−555; MRC 2322−052; MRC 0355−037) of HzRG fields. The new IRAC maps are composed of a 4×3 grid of pointing positions, and at each position there are 15 dithered frames of 100 s exposure time each. The new MIPS maps are comprised of a 6×6 grid of pointing positions, and with each position mapped twice with an individual 30-s exposure time.

From the Spitzer Science Center's basic calibrated data (BCD) frames we build mosaics for each field using a customized IDL package (Gutermuth et al. 2008). A number of common bright source artefacts (banding, jailbars, muxbleed, and pulldown effects) are corrected in the individual BCD frames as a first step. Then the code rejects the transients and accounts for distortions introduced by rotation and subpixel offsets in building the mosaics. One additional calibration step, performed only on the MIPS observations, is a self-calibration to remove systematic artefacts (like bright and dark latents) from the maps. For each MIPS astronomical observation request (AOR), a flat-field map is made by taking the median of the background at each BCD pixel. Then the median background map is normalized, and all the BCD images for that AOR are divided by the normalized flat-field map. The final calibrated, corrected mosaics for IRAC and MIPS were then resampled to a scale of 0.865 and 1.80 arcsec pixel^{-1}, respectively.

Photometric measurements were performed on the mosaics using the IDL routine APER with an aperture diameter of 3.8 arcsec. We apply aperture corrections in the IRAC bands of [1.40, 1.38, 1.55, 1.70], and for MIPS we use a correction of 2.00. The corrections are determined by selecting isolated sources, having no neighbouring detection at 5σ within 10 arcsec identified by Source Extractor (Bertin & Arnouts 1996), and taking the ratio of the fluxes of those isolated sources with apertures of 12.4 and 3.8 arcsec diameter. The differences between our aperture corrections and those listed in the IRAC Instrument Handbook are as one would expect for our 3.8 arcsec diameter photometry aperture. For each map the median of these flux ratios is taken, and then the overall aperture correction is chosen as the mean of the set of corrections derived for each band. Small field-to-field variations in the median aperture corrections introduce some systematic uncertainties in our photometry, and so the standard deviation of the aperture corrections derived in our maps is added in quadrature to the statistical photometric errors for the *Spitzer* bands. In the event that we do not detect an active galaxy, we give a 3σ upper limit.

10 of the radio galaxies in our sample have *Spitzer* photometry reported in the literature (Villar-Martín et al. 2006; Seymour et al. 2007). For all but one of these (PKS 0529-549), our photometry is consistent with the previously published measurements. In the case of PKS 0529-549, we measure the 24-μm flux and find the value to be significantly lower than that reported by Seymour et al. (2007): we obtain 632 ± 27 μJy compared to the 942 ± 71 μJy of Seymour et al. (2007). The higher flux density obtained by Seymour et al. is probably due to the presence of a second 24-μm source located ∼6 arcsec south-west of the radio galaxy, which would have contributed significantly to the light measured in their relatively large 13-arcsec diameter aperture, but significantly less so in our 3.8-arcsec aperture.

3 RESULTS

Figs 1 and 2 show $160 \times 160 \, \text{arcsec}^2$ 'postage stamps' cut out from the full-size signal-to-noise ratio maps, with contours starting at 2σ and increasing linearly by 1σ. Bars indicate the orientation of the radio source, where applicable. Most of the active galaxies in our sample have been observed at a variety of wavelengths and spatial resolutions, meaning that there are various different ways by which one can define the position of the galaxy. For this study, we will adopt the coordinates that are most likely to mark the position of the galactic nucleus. Our preferred position is that of the radio core, since it corresponds to the active nucleus itself. For active galaxies for which the radio core has not been detected, or which are radio quiet, our second choice is to use the centroid of the *Spitzer* IRAC emission, averaged across the 3.6- and 4.5-μm bands. For type 2 (i.e. narrow line) objects this emission is expected to trace the evolved stellar population, which is likely to be more dynamically relaxed than young stellar populations which, if present, could dominate at shorter optical–IR and longer (i.e. MIPS) wavelengths. For type 1 (broad line) objects, this emission is likely to be dominated by the active nucleus. Finally, in the absence of both a radio core detection and IRAC data, we adopt the position of the optical or near-IR emission. The postage stamp images are centred on our fiducial 'radio-optical' position, the coordinates of which are listed in Table 1.

3.1 Association between millimetre sources and radio galaxies

In this paper we adopt a source detection threshold such that the peak S/N is ≥ 3.0 and also that the spatial full width at half-maximum (FWHM) is consistent with, or larger than, the FWHM of the filtered point spread function (i.e. FWHM ≥ 34 arcsec). We have attempted to identify sources associated with our active galaxies as follows. First, we have calculated the Poisson probability that a detected millimetre source is merely a chance association, rather than being associated with the active galaxy. This is given by

$$P = 1 - e^{-\pi r^2 N}, \tag{1}$$

where r is the angular distance of the millimeter source from the optical/IR/radio position of the active galaxy, and N is the surface density of millimeter sources in blank fields that have 1.1-mm flux densities greater than or equal to that of the detected millimeter source (Downes et al. 1986). For N we adopt the number counts from the AzTEC/SHADES survey (Austermann et al. 2010). We consider a millimeter source to be associated with the active galaxy when the *P*-statistic is less than 0.05, i.e. the null hypothesis of chance association is significant at the <5 per cent level. All 17 of the active galaxies in our sample have at least one associated 1.1-mm source.

However, we must apply an additional criterion in order to determine whether any of the associated millimeter sources is consistent with being at the position of the active galaxy. In other words, are the optical/IR/radio and millimeter positions consistent, taking into
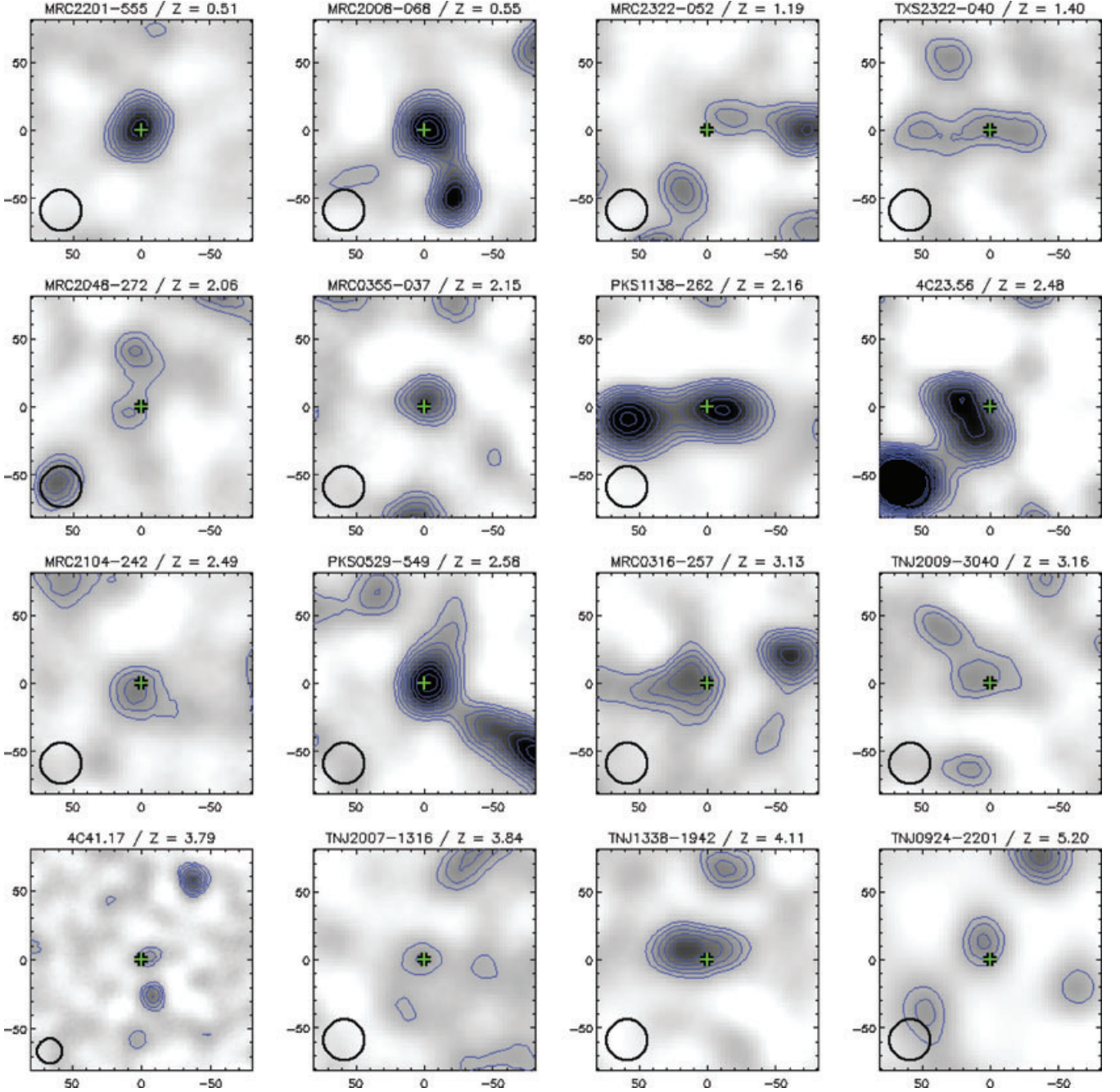
Figure 1. Postage stamps of 1.1-mm AzTEC signal-to-noise ratio maps for the 16 radio galaxies, which show a $160 \times 160 \, \text{arcsec}^2$ field (or $0.9 \times 0.9 \, \text{Mpc}$ to $1.4 \times 1.4 \, \text{Mpc}$ in physical units) centred on the radio-optical position ($+$). Both axes are labelled in arcsec, with the spatial zero corresponding to the radio-optical position of the radio galaxy. The galaxies are ordered with z increasing left to right, top to bottom. Contours start at 2σ and increase linearly by 1σ. The FWHM of the beam is shown in the lower-left corner of each map. Note that the map of 4C+41.17 has a smaller beam FWHM than the rest of the sample, because the observations were made using the 15-m JCMT (beam FWHM = 18 arcsec), rather than the 10-m ASTE (beam FWHM = 28 arcsec). Probable 1.1-mm counterparts for 10 of the radio galaxies are detected at $\geq 3\sigma$ significance.

account the observational errors in the position of the millimeter source? The 1σ positional error of an observed millimeter source is

$$\sigma_{\text{pos}} \simeq \sqrt{\left(\frac{0.6 FWHM}{\text{S/N}_d}\right)^2 + \sigma_{\text{pnt}}^2} \,, \qquad (2)$$

where FWHM is that of the filtered beam, S/N_d is the *de-boosted* signal-to-noise ratio of the millimetre counterpart, and σ_{pnt} is

the 1σ uncertainty in the pointing of the map (adapted from Ivison et al. 2007). We conservatively assume that $\sigma_{\text{pnt}} \sim 1$ arcsec (Scott et al. 2010). As an illustration, a source with $\text{S/N}_d = 3.0$ would have a positional error $\sigma_{\text{pos}} \simeq 6.9$ arcsec. Note that equation (2) does not take into account any systematic absolute offset in the map, i.e. residuals after pointing corrections.

We classify an AzTEC source as the 1.1-mm counterpart to the radio galaxy or quasar when $P < 0.05$ and when the spatial offset
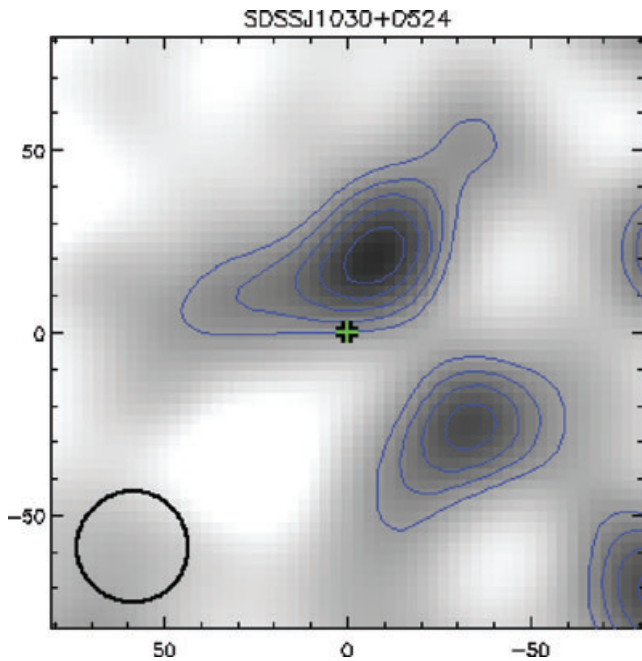
Figure 2. Postage stamp of the 1.1-mm AzTEC signal-to-noise ratio map for the $z = 6.3$ radio-quiet quasar SDSS J1030+0524. The 160×160 arcsec^2 field (or 0.9×0.9 Mpc^2 in physical units) is centred on the optical position, which is marked by a cross. Contours start at 2σ and increase linearly by 1σ. The FWHM of the beam is shown in the lower left corner. We do not detect the 1.1-mm counterpart of this galaxy.

from the radio-optical position r is less than $2.7\sigma_{pos}$.[1] There are 11 AzTEC sources that satisfy our criteria for classification as 1.1-mm counterparts to the radio galaxies or quasar. Note that six active galaxies have both $P \leq 0.05$ and $r > 2.7\sigma_{pos}$: this means they have a statistically significant association with a millimetre galaxy which is not likely to be the active galaxy host. The results from this analysis are shown in Table 1.

Finally, while the presence of other (bright) sources within $\sim$30–60 arcsec can potentially skew the centroid of a millimetre source due to the negative sidelobes of the telescope beam, our tests show that this effect is negligible for our entire sample: all such centroid shifts are ≤ 1 arcsec and do not affect our counterpart versus non-counterpart classification.

3.2 Consistency with previous millimetre/submillimetre measurements

A number of the galaxies in our sample have been imaged previously at millimetre or submillimetre wavelengths. These are 4C+41.17 (Ivison et al. 2000; Stevens et al. 2003; Greve et al. 2007), PKS 1138−262 (Stevens et al. 2003), TN J1338−1942 (De Breuck et al. 2004) and SDSS J1030+0524 (Priddey, Ivison & Isaak 2008). Taking into account the (usually) lower spatial resolution of our new observations, we find a good agreement with the images and photometry from the literature. In two cases (PKS 1138−262 and TN J1338−1942), several discrete sources detected by SCUBA or MAMBO are blended together in our images, due to their relatively lower spatial resolution.

In addition, eight of our sample have been targeted with SCUBA photometry (4C+23.56, 4C+41.17: Archibald et al. 2001; PKS

1138−262, MRC 0316−257, TN J2007−1316, TN J1338−1942, TN J0924−2201: Reuland et al. 2004; SDSS 1030+0524: Priddey et al. 2003). For seven of these galaxies, we find a good agreement between our flux density measurements and the SCUBA photometry. (We use a scaling factor of 2.5 between 850 μm and 1.1 mm, assuming $T_{dust} = 40$ K and $\beta = 1.5$; see Section 3.5.)

TN J0924−2201 is the exception. Reuland et al. (2004) derived a 3σ limit of ≤ 3.2 mJy at 850 μm, which implies a 1.1-mm flux density of $\lesssim 1.3$ mJy, whereas we determine the 1.1-mm flux density of 3.6 ± 0.9 mJy. The reason for this discrepancy is not clear. It may suggest that the 1.1-mm source we identify with the radio galaxy is not the true 'counterpart', and instead is a companion MMG offset from the position of the radio galaxy host (see Section 6). Maps with higher spatial resolution and S/N will be needed to address this issue.

3.3 Stacking

Next we derive average values of $S_{1.1}$ for various subsets of our sample. To do this we stack the AzTEC images at the position of the active galaxy, allowing us to include information from the individual observations wherein the active galaxy counterpart was not detected at $\geq 3\sigma$ significance. First, we spatially registered the images. In the case of 4C +41.17, we resampled the image to a scale of 3 arcsec pixel^{-1}. Next, we assigned to each image a weighting proportional to σ^{-2}. We then stacked all the images in our sample (Fig. 3, top left). From this stacked image, we determine an average $S_{1.1} = 3.4 \pm 0.2$ mJy at the position of the active galaxy. We repeat this using only the radio galaxy images, and obtain an average $S_{1.1} = 3.2 \pm 0.2$ mJy (Fig. 3, top right). Repeating for the six active galaxies for which we did not detect a millimetre counterpart, we obtain an average flux density $S_{1.1} = 2.0 \pm 0.3$ mJy (Fig. 3, middle left). Finally, for the five undetected radio galaxies we stack to obtain an average flux density $S_{1.1} = 2.4 \pm 0.3$ mJy (Fig. 3, middle right).

We have also investigated whether the millimetre emission is more extended along the radio axis of the radio galaxies in our sample. This is motivated in part by the fact that the ultraviolet and optical emission from powerful radio galaxies is usually aligned with the radio source (e.g. Chambers, Miley & van Breugel 1987; McCarthy et al. 1987), and the apparent alignment between the radio source and the large-scale distribution of MMGs found by Stevens et al. (2003) in a sample of seven radio galaxies at $2.2 \leq z \leq 4.3$. To this end, the AzTEC images were registered, rotated such that the radio axis runs horizontally, and subsequently stacked (Fig. 3, bottom left). Along the radio axis in the stacked image, we obtain FWHM = 39.3 ± 0.6 arcsec, compared to FWHM = 40.8 ± 0.6 arcsec determined orthogonally to the radio axis. Thus, we conclude that there is no significant trend for the millimetre emission to be more elongated along the radio axis than it is along the orthogonal axis, at least at the spatial resolution of our observations.

3.4 Synchrotron emission

Before using the 1.1-mm flux densities to estimate the infrared luminosity and the implied rate of star formation, we must first consider the impact of synchrotron emission from the radio source at 1.1 mm. Indeed, previous studies have shown that in some high-z radio galaxies, the synchrotron emission has sufficiently high luminosity and/or a sufficiently flat SED at high frequencies to be detectable in the millimetre-wave regime (e.g. Archibald et al. 2001; Vieira et al. 2010).

---

[1] The positional error distribution is non-Gaussian. $2.7\sigma_{pos}$ corresponds to a 95 per cent cumulative probability.

Table 1. Basic properties of the sample of radio galaxies. Columns are as follows. (1) Name of the active galaxy. (2) Active galaxy redshift. (3) Rest-frame wavelength, in the unit of μm, corresponding to 1.1 mm in the observer frame. (4) and (5) are the RA and Dec. of the active galaxy. (6) The wavelength regime from which the position of the active galaxy was determined, where R = radio, I = mid-IR (3.6 and 4.5 μm), O = optical (*R* band) and K = near-IR (*K* band). (7) 1.1-mm flux density of the millimetre counterpart to the active galaxy. Errors in $S_{1.1}$ are 1σ, and upper limits are 3σ. (8) The observed offset of the millimetre counterpart relative to the position of the active galaxy. In the absence of a probable counterpart we show in parentheses the offset to the closest millimetre detection. (9) *P*-statistic of the probable millimetre counterpart. Again, in the absence of a probable counterpart we show in parentheses the *P*-statistic of the nearest millimetre detection. (10) Log of the far-IR luminosity of millimetre counterparts. For non-detections, we give 3σ upper limits. (11) The star formation rate implied by the far-IR luminosity. Included at the bottom of the table is the radio-quiet quasar SDSS J1030+0524.

Source name	z	$\lambda_{\rm rest}$ (μm)	RA (J2000) (hh:mm:ss.ss)	Dec. (J2000) (dd:mm:ss.s)	ID	$S_{1.1}$ (mJy)	r (arcsec)	P	Log ($L_{\rm FIR}/L_\odot$)	SFR ($M_\odot$ yr^{-1})
(1)	(2)	(3)	(4)	(5)	(6)	(7)	(8)	(9)	(10)	(11)
MRC 2201−555	0.51	730	22:05:04.83	−55:17:44.0	I	6.1±0.8	2.5	8×10^{-6}	12.86	720
MRC 2008−068	0.55	710	20:11:14.22	−06:44:03.6	R	8.6±0.9	3.5	4×10^{-6}	13.04	1100
MRC 2322−052	1.19	500	23:25:19.62	−04:57:36.6	I	<2.1	(20.7)	(0.049)	<12.60	<400
TXS 2322−040	1.51	440	23:25:10.23	−03:44:46.7	R	2.3±0.6	2.3	0.0006	12.68	480
MRC 2048−272	2.06	360	20:51:03.49	−27:03:03.7	I	2.3±0.8	11.4	0.02	12.68	480
MRC 0355−037	2.15	350	03:57:48.06	−03:34:09.5	I	3.5±0.7	6.6	0.002	13.02	1040
PKS 1138−262	2.16	350	11:40:48.35	−26:29:08.6	R	<3.6	(14.3)	(0.007)	<12.85	<710
4C +23.56	2.48	320	21:07:14.82	+23:31:45.1	R	<1.5	(21.4)	(0.005)	<12.46	<290
MRC 2104−242	2.49	320	21:06:58.27	−24:05:09.1	R	3.7±0.9	6.9	0.002	12.87	740
PKS 0529−549	2.58	310	05:30:25.43	−54:54:23.3	I	6.4±0.7	3.7	2×10^{-5}	13.10	1270
MRC 0316−257	3.13	270	03:18:12.14	−25:35:10.2	I	<2.1	(17.3)	(0.009)	<12.55	<350
TN J2009−3040	3.16	260	20:09:48.08	−30:40:07.4	K	3.3±0.9	12.9	0.005	12.79	610
4C +41.17	3.79	230	06:50:52.35	+41:30:31.4	O	3.5±1.0	6.6	0.001	12.78	610
TN J2007−1316	3.83	230	20:07:53.22	−13:16:43.4	R	2.8±0.9	4.0	0.002	12.68	480
TN J1338−1942	4.10	220	13:38:26.23	−19:42:33.6	R	<5.0	(15.7)	(0.0008)	<12.90	<790
TN J0924−2201	5.19	180	09:24:19.91	−22:01:41.5	I	3.6±0.9	13.9	0.006	12.74	560
SDSS J1030+0524	6.28	150	10:30:27.10	+05:24:55.0	I	<1.4	(22.7)	(0.02)	<12.30	<200

To quantify the possible contribution at 1.1 mm from synchrotron emission $S_{\rm ext}$, we have extrapolated a power law of the form $S_v \propto v^{\alpha_{\rm rad}}$ from the two highest frequency photometric data points of the observed radio spectra separated in v by a factor of ≥ 1.2. When more than one measurement is available at 'similar' frequencies, which we define as when the ratio between frequencies is ≤ 1.2, we have conservatively used the measurement that would result in the highest value of $S_{\rm ext}$ (e.g. MRC 0355−037). In Fig. 4. we show the radio–IR spectral energy distributions of the radio galaxies in our sample, including our extrapolations to 1.1 mm of the synchrotron emission.

In the first instance, we have used radio photometric measurements that represent flux densities integrated across the entire spatial extent of the radio source, as these data are readily available for all of the radio galaxies in our sample. However, extrapolating the radio lobe SED to the millimetre regime is less than ideal. With the possible exceptions being the two smallest radio galaxies (MRC 2008−068 and TXS 2322−040), this photometry is dominated by the extended radio lobes (see e.g. Carilli et al. 1997; Pentericci et al. 2000). Lobe spectra usually steepen towards higher frequencies (e.g. Muxlow, Pelletier & Roland 1988; Murgia et al. 1999); therefore, in most cases this extrapolation is expected to overpredict the contribution from the extended lobes, that is, $S_{\rm ext}$ is expected to represent an extreme upper limit to the contamination due synchrotron emission from the lobes. Table 2 gives $S_{\rm ext}$ alongside $S_{1.1}$, $\alpha_{\rm rad}$, and the radio wavelengths used for the extrapolations. The table also gives references to the photometric data points plotted in Fig. 4.

All 11 of the radio galaxies which we have detected at 1.1 mm have $S_{1.1}$ measurements exceeding $S_{\rm ext}$. This means that synchrotron emission from the radio lobes clearly cannot be responsible for all

of the 1.1-mm emission from these radio galaxies. Although for six of those 11 radio galaxies $S_{\rm ext}$ is greater than the 1σ uncertainty on $S_{1.1}$, we refrain from drawing the naive conclusion that $S_{1.1}$ in some cases may be significantly enhanced by synchrotron emission, because our extrapolation of $S_{\rm ext}$ is based on a very favourable set of assumptions, and the results thereof represent rather extreme upper limits. Indeed, in one particular case (MRC 0316−257) $S_{\rm ext}$ is actually a factor of ∼2 *higher* than the 3σ lower limit to $S_{1.1}$.

Moving into the millimetre regime from the radio, the flux density of the lobes diminishes more rapidly than that of the core (e.g. Carilli et al. 1997) so that at millimetre wavelengths the core typically dominates the spatially integrated synchrotron flux density (see, e.g. fig. 1 of Nesvadba et al. 2009; Downes et al. 1996). Thus, we must also consider whether the radio core might contribute significantly to the 1.1-mm emission. The radio core has been detected in only four of our radio galaxy sample (Chambers et al. 1996; Carilli et al. 1997; Pentericci et al. 2000, 2001), and for these galaxies we have extrapolated the radio core SED to 1.1 mm using a power law. One of these galaxies was detected at 1.1 mm (MRC 2104−242), and the value of $S_{\rm ext}$ for its core is several orders of magnitude below our $S_{1.1}$ measurement (and well below the $S_{\rm ext}$ extrapolated from the radio lobes).

In summary, the radio lobes are unable to provide sufficient synchrotron flux at 1.1 mm to be responsible for the flux densities we obtain at that wavelength, despite our use of a very favourable set of assumptions. Furthermore, it seems likely that any enhancement by synchrotron emission is smaller than the 1σ uncertainty in our flux density measurements, i.e. insignificant, in essentially all cases. Thus, we prefer not to apply any correction for synchrotron contamination to our obtained values of $S_{1.1}$, because the extrapolation of the synchrotron flux density is so uncertain. Finally, we
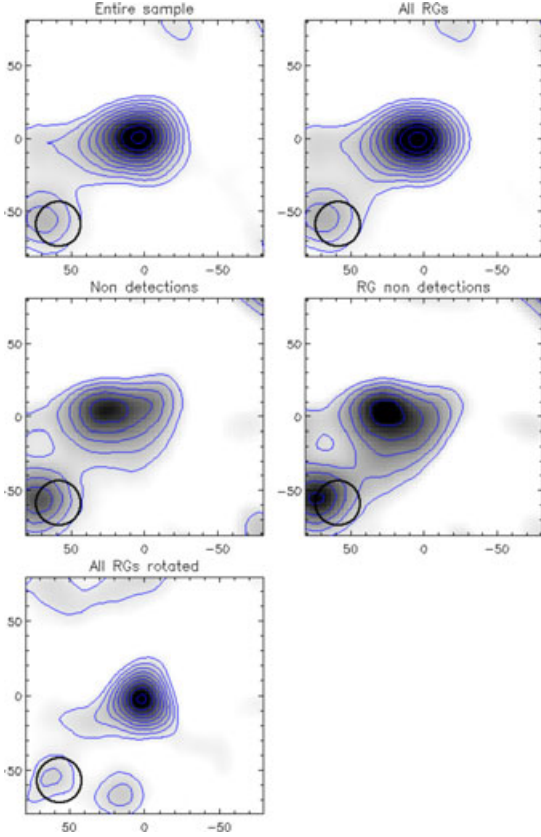
Figure 3. Postage stamps of the stacked AzTEC images. The images were shifted such that the radio-optical position of the active galaxy is at the centre, and then co-averaged with weightings proportional to σ^{-2}. Top left: all the 17 active galaxies in our sample. Top right: all the 16 radio galaxies. Middle left: all non-detections. Middle right: non-detected radio galaxies. Bottom left: radio galaxies stacked with their radio source axes running horizontally. Contours begin at 2σ, and increase linearly by 2σ.

comment that the issue of possible synchrotron contamination would be resolved with observations at longer millimetric wavelengths (e.g. 2–3 mm).

3.5 Implied star formation rates

In order to convert our obtained flux densities into far-IR luminosities (L_{FIR}) and star formation rates (SFRs), we adopt a grey-body emission template with an emissivity index β and a dust temperature T_{dust}. This gives

$$M_{dust} = \frac{S_{obs} D_L^2}{(1+z)\kappa_{\nu_{rest}} B_{\nu_{rest}}(T_{dust})}, \tag{3}$$

$$L_{FIR} = \frac{8\pi h \kappa_{\nu_{rest}}}{c^2 \nu^\beta} \left(\frac{kT_{dust}}{h}\right)^{\beta+4} \Gamma(\beta+4)\zeta(\beta+4)M_{dust}, \tag{4}$$

$$SFR = \frac{L_{FIR}}{10^{10} L_\odot} \, M_\odot \, yr^{-1}, \tag{5}$$

where M_{dust} is the mass of dust, S_{obs} is the observed flux density, D_L is the luminosity distance, $\kappa_{\nu_{rest}}$ is the mass absorption coefficient of the dust at rest-frame frequency ν_{rest}, and $B_{\nu_{rest}}(T_{dust})$ is the Planck function at ν_{rest} (e.g. Archibald et al. 2001). Γ is the Gamma function and ζ is the Riemann zeta function. A Salpeter initial mass function has been assumed. Throughout this paper, we assume $T_{dust} = 40$ K,

$\beta = 1.5$ (after Archibald et al. 2001). We adopt $\kappa_{375\,GHz} = 0.15$ m^2 kg^{-1} (Hildebrand 1983), and extrapolate to other frequencies assuming $\kappa_\nu \propto \nu^\beta$ (Chini, Krügel & Kreysa 1986).

The values we have obtained for $S_{1.1}$ imply SFRs ranging from <200 to ~1210 M$_\odot$ yr^{-1}. The sample-averaged $S_{1.1}$ we obtained from our stacking analysis implies an average SFR $\sim$ 600 M$_\odot$ yr^{-1}.

4 COMPARISON WITH RADIO AND OPTICAL PROPERTIES

4.1 Anticorrelation between $S_{1.1}$ and radio source size

It is interesting to examine what, if any, relationship there might be between millimetre/submillimetre flux density measurements and the radio source size. This is motivated by a number of relatively recent observational results suggesting that the presence of intense star-formation in high-z radio-loud galaxies is anticorrelated with the size of the radio source (Best, Longair & Röttgering 1996; Willott et al. 2002; Humphrey et al. 2006).

For the purpose of this analysis, we define radio source size as the largest projected extent of the radio emission: we have determined the largest angular extent from published radio images, using high spatial resolution images wherever possible. Whenever possible we use high spatial resolution images (FWHM $\lesssim 0.5$ arcsec). For sources which are not well resolved, or which do not have a radio image published in the literature, we adopt the largest angular size, or the upper limit thereto, listed in the literature. Angular sizes were converted to physical units of kpc, using the conversion dictated by our preferred cosmology.

For high-z radio galaxies, the published radio images tend to be sensitive enough only to detect the relatively compact and high surface brightness parts of the radio source, i.e. hotspots and the core. Therefore, in classical double/triple radio galaxies, the largest angular size typically represents the angular distance between the most distant hotspot, relative to the nucleus, in each of the two jets. It is important to be aware that it is quite possible that radio-emitting structures too faint to be detected lie yet farther from the nucleus (see e.g. Coma A: van Breugel et al. 1985; 3C171: Blundell 1996; B3 J2330+3927 at $z = 3.087$: Pérez-Torres & De Breuck 2005). In this case, our obtained radio source sizes would underestimate the true size. While we clearly cannot ascertain whether the hotspot separations are genuinely representative of the total radio source sizes in our high-z sample, we find it encouraging that in low-z powerful radio galaxies the hotspot separation is usually representative of the total angular extent (see e.g. Black et al. 1992).

In Fig. 5 we plot $S_{1.1}$ versus the size of the radio emission for our sample. We find an L-shaped anticorrelation between $S_{1.1}$ and radio size. The three galaxies with the highest values of $S_{1.1}$ (≥ 5 mJy: MRC 2201$-$555; MRC 2008$-$068; PKS 0529$-$549) have relatively small radio sources (≤ 22 kpc), while those with relatively large radio sources (>22 kpc) all have relatively low $S_{1.1}$ (≤ 5 mJy). To test the significance of this apparent anticorrelation in our AzTEC sample, we use Cox's proportional hazard model (Isobe, Feigelson & Nelson 1986), which is able to treat censored data, i.e. upper limits. Using the null hypothesis that no correlation is present between $S_{1.1}$ and radio size, we obtain a global $\chi^2 = 8.3$, which corresponds to a significance level for independence of 0.003. Thus, the anticorrelation is highly significant.

An alternative test can be made via Poisson probability theory. In this case we adopt a null hypothesis such that the population of
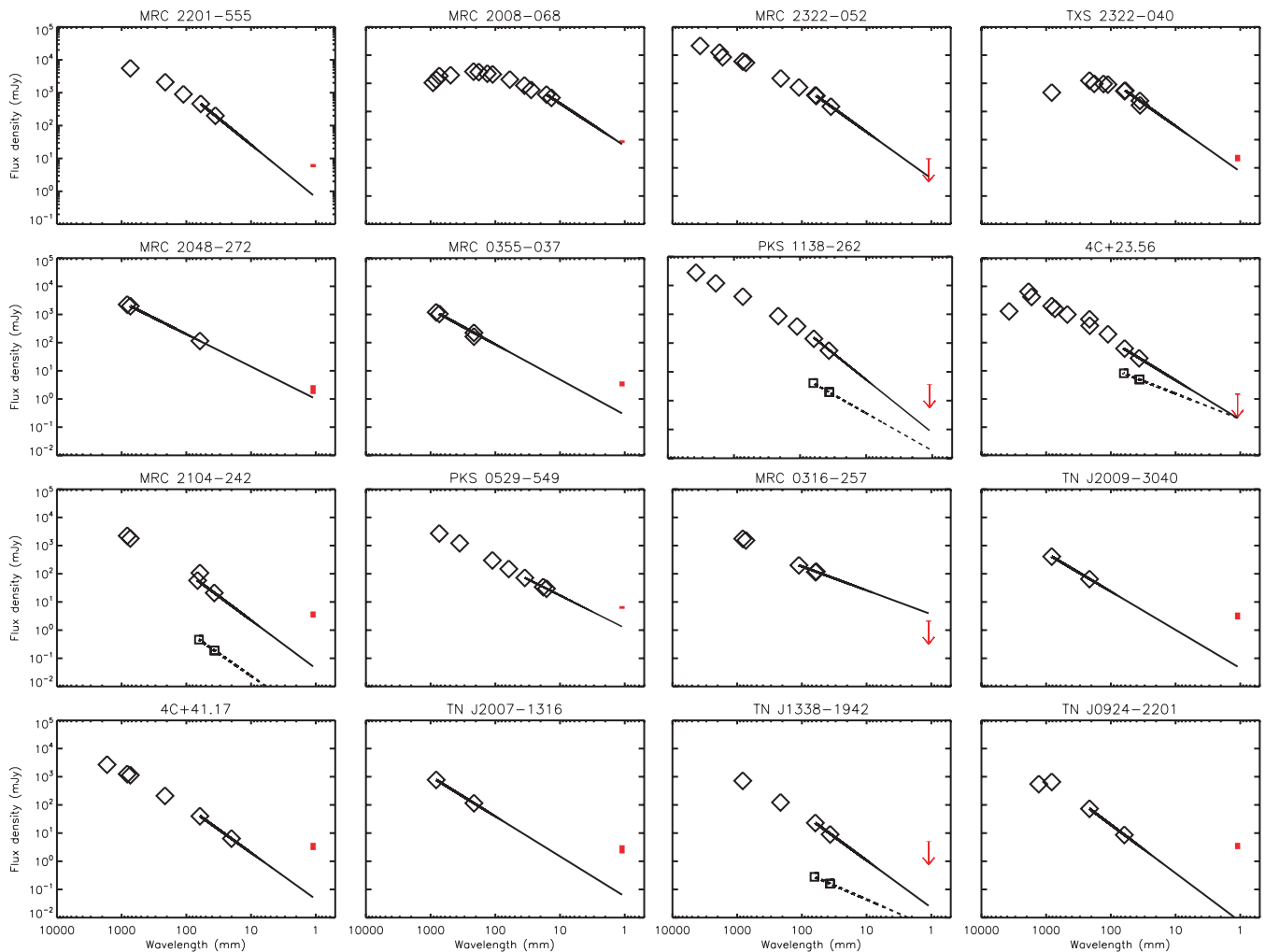
Figure 4. The observer-frame radio spectral energy distributions of the radio galaxies in our sample and our extrapolation therefrom of extreme upper limits on the 1.1-mm flux density due to synchrotron emission. The red vertical bars show our AzTEC 1.1-mm flux density measurement, with the vertical length indicating the range of values permitted by the 1σ uncertainty. Where we have not detected the radio galaxy's millimetre counterpart, we instead mark its 3σ upper limit with a red arrow. Black diamonds show flux density measurements of the synchrotron emission, integrated over the entire radio source. The solid line is our power-law extrapolation of this emission from the high-frequency radio regime to 1.1 mm. Where a galaxy's radio core has been detected at more than one radio frequency, its flux density measurements are represented by black squares. Our power-law extrapolation of the radio core SED to 1.1 mm is shown by the dashed black line. References to the radio measurements from the literature are given in Table 2.

radio galaxies with relatively large radio sources (>50 kpc) has the same fraction of galaxies with $S_{1.1} \geq 5$ mJy as does the population of radio galaxies with relatively small radio sources (≤ 50 kpc). In our sample, there are three radio galaxies with $S_{1.1} \geq 5$ mJy and $D_{radio} \leq 50$ kpc; there are three with $S_{1.1} < 5$ mJy and $D_{radio} \leq 50$ kpc; there are 10 with $S_{1.1} < 5$ mJy and $D_{radio} > 50$ kpc; and there is none with $S_{1.1} \geq 5$ mJy and $D_{radio} > 50$ kpc. Under the null hypothesis, the probability of counting 0 radio galaxies with $S_{1.1} \geq 5$ mJy and $D_{radio} > 50$ kpc is 4.5×10^{-5}. Therefore, we reject the null hypothesis, and conclude that the AzTEC radio galaxy sample shows a highly significant anticorrelation between the 1.1-mm flux density and the apparent size of the radio source.

Shown in Fig. 6 is $S_{1.1}$ versus radio size for the AzTEC counterparts together with HzRGs that have been observed at 850 μm using SCUBA (Archibald et al. 2001; Reuland et al. 2003b, 2004; Stevens et al. 2003). SCUBA 850-μm flux densities have been scaled by 1/2.5 to extrapolate their 1.1-mm flux densities. This scaling factor is calculated assuming $T_{dust} = 40$ K and $\beta = 1.5$ (Section 3.5). Where an HzRG has been observed more than once

at 1.1 mm and/or 850 μm, we use the most sensitive of the flux density measurements. Using Cox's proportional hazard model we find that this combined data set does not show a significant anticorrelation between $S_{1.1}$ or SFR and radio size ($P = 0.18$), in agreement with the statistical analysis of Reuland et al. (2004). However, using Poisson probability theory we find that the absence of HzRGs at $S_{1.1} \geq 2.5$ mJy and $D_{radio} > 200$ kpc is significant at the 98 per cent level ($P = 0.02$).

It seems plausible that this reduction in the significance of the trend is due to the different observational methods employed in our AzTEC/ASTE survey of HzRGs, compared to those predominantly used for the several SCUBA/JCMT surveys. Whereas our maps allow us to reject sources that are close to the radio galaxy's position but unlikely to be the counterpart, the SCUBA photometry employed by Archibald et al. (2001) and Reuland et al. (2004) simply obtains the flux density from a region of sky sampled by the telescope beam, and emission from a bright nearby companion MMG may contaminate such measurements, thereby adding scatter to the trend.

Table 2. Extrapolation of a power law from radio to millimetre wavelengths. The columns are organized as follows. (1) Name of the radio galaxy; if the radio core has been detected at more than one radio wavelength, it is also included in this table. (2) Redshift z of the radio galaxy. (3) Observed flux density of the radio galaxy's 1.1-mm counterpart. (4) The extrapolated 1.1-mm flux density of the integrated radio source, or radio core where appropriate. (5) Radio spectral index of the integrated radio source, or the radio core where appropriate. (6) and (7) The wavelengths of the two radio photometric data points used in the extrapolation. (8) References to photometric data from the literature which we have used in this paper; references have been abbreviated to the first two letters of the first author's surname and the last two digits of the publication year; the abbreviations are appended to their corresponding full references at the end of this paper.

| Source name	z	$S_{1.1}$ (mJy)	S_{ext} (mJy)	α_{rad}	λ_1 (cm)	λ_2 (cm)	Radio data references
(1)	(2)	(3)	(4)	(5)	(6)	(7)	(8)
MRC 2201-555	0.51	6.1 ± 0.8	0.8	-1.60	3.6	6.0	La81 Wr90 Wr94 Gr94 Bu06
MRC 2008-068	0.55	8.6 ± 0.9	6.9	-1.51	1.4	1.6	Bo75 Ku81 Wr90 Gr95 Do96 Co98 St98 St05 Ri06a,b He07
MRC 2322-052	1.19	<2.1	0.2	-1.65	3.6	6.0	Go67 La81 Wr90 Wh92 Gr95 Sl95 Do96 Co98 Co07
TXS 2322-040	1.51	2.3 ± 0.6	0.9	-1.62	3.6	6.0	Wr90 Wh92 Gr95 Do96 Co98 Xi05 Xi06 Li07
MRC 2048-272	2.06	2.3 ± 0.8	1.1	-1.15	6.2	73.4	La81 Gr94 Do96 Pe00 Se07
MRC 0355-037	2.15	5.0 ± 0.8	0.3	-1.25	21.4	73.4	La81 Wh92 Do96 Co98 Co07
PKS 1138-262	2.16	<3.6	0.09	-1.84	3.7	6.4	La81 Wr90 Gr94 Sl95 Do96 Ca97 Co07 Co98 Re04
PKS 1138-262 core		0.02	-1.3	3.7	6.4	Ca97	
4C +23.56	2.48	<1.5	0.2	-1.4	3.7	6.4	Pi65 Fa74 Wr90 Gr90 Gr91 Be91 Wh92 Sl95 Do96 Ca97 Co07
4C+23.56 core		0.2	-0.9	3.7	6.4	Ch96 Ca97	
MRC 2104-242	2.49	3.7 ± 0.9	0.05	-1.71	3.7	6.7	La81 Gr94 Do96 Pe00 Co07
MRC 2104-242 core		0.0007	-1.6	3.7	6.7	Pe00	
PKS 0529-549	2.58	6.4 ± 0.7	1.3	-1.15	1.6	3.5	La81Wr90 Gr94 Wr94 Ma03 Br07
MRC 0316-257	3.13	<2.1	4.0	-0.85	6.0	11.1	La81 Wr90 Gr94 Do96 Re04 Co07
TN J2009-3040	3.16	3.3 ± 0.9	1.1	-1.34	6.2	21.4	Do96 DeBr00
4C +41.17	3.79	3.5 ± 1.0	0.05	-1.65	2.0	6.1	Go67 Vi75 Fi85 Ch90 Gr91 Be91 Wh92 Ha93 Do96 Ch96 Be99 Gr07 Co07
TN J2007-1316	3.83	2.8 ± 0.9	1.7	-1.42	21.4	82.0	La81 Do96 DeBr00 Re04
TN J1338-1942	4.10	<5.0	0.02	-1.68	3.7	6.4	Do96 Re04 DeBr00 DeBr04 Do07
TN J1338-1942 core		0.004	-1.0	3.7	6.4	DeBr00 Pe00	
TN J0924-2201	5.19	3.6 ± 0.9	0.01	-1.72	6.2	21.4	Do96 vB99 DeBr00 Re04 Ca07
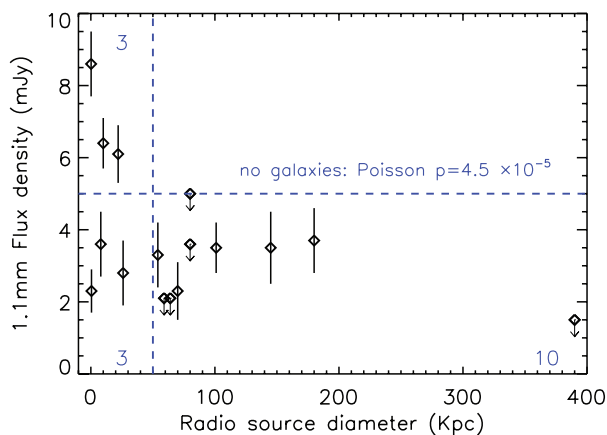
Figure 5. The anticorrelation between 1.1-mm flux density and radio source diameter in our AzTEC sample. The dashed lines show the divisions used to calculate the Poisson probability

Figure 6. Similar to Fig. 5, but including also HzRGs with measurements or limits at 850 μm. We have extrapolated 850-μm flux densities to 1.1 mm by multiplying by 1/2.5. To avoid complicating the figure, error bars are not shown.

Finally, we point out that the trend discussed above would not change significantly if we were to include only millimetre/submillimetre measurements obtained from maps (e.g. from Ivison et al. 2000; Stevens et al. 2003; De Breuck et al. 2004; Greve et al. 2007; and this paper), i.e. excluding measurements obtained from simple SCUBA photometry. We would still find that, of the radio galaxies with radio sources smaller than 200 kpc, 50 per cent have $S_{1.1} < 5$ mJy, while the radio galaxies with radio sources larger than 200 kpc all have $S_{1.1} < 5$ mJy. In Section 6 we discuss the origin and implications of this result.
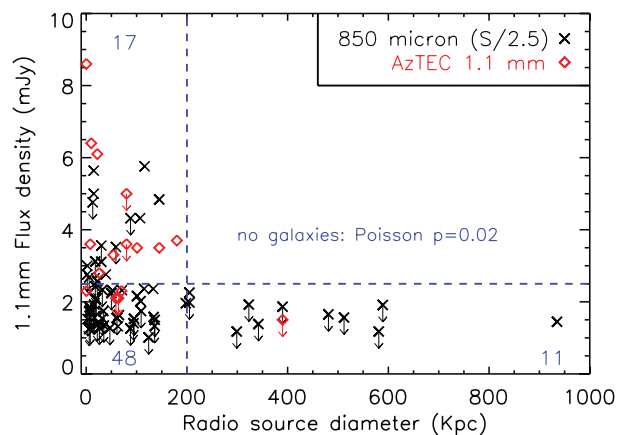
4.2 The Lyα emission nebulae

In addition to heating the surrounding dust young stars also produce H II regions, which emit strong UV–optical emission lines. The strongest of these lines is Lyα λ1216, and its luminosity is primarily a function of the number of ionizing photons absorbed, and the quantity and geometry of dust. It is relatively insensitive to the metallicity or the gas density of the H II regions. Thus, Lyα carries useful information about dust associated with star-forming regions.

Table 3. Radio and optical properties of the radio galaxies. A dash (–) indicates that a quantity has not yet been determined, or is not available in the literature. Columns are as follows. (1) Source name. (2) Source redshift. (3) The 1.1-mm flux density of the millimetre counterpart, obtained from our AzTEC data. (4) The spectroscopic Lyα luminosity in the unit of 10^{44} erg s^{-1}. (5) Lyα luminosity in the unit of 10^{44} erg s^{-1} obtained from narrow-band images. (6) The flux ratio Lyα/He II. (7) Ratio of the Lyα luminosity to the far-infrared luminosity; the theoretically expected value is ~0.03; Lyα luminosities obtained from narrow-band images are used where available, otherwise luminosities obtained from long-slit spectra are used. (8) Projected size of the radio source (D_{radio}). (9) References for the size of the radio source, and for the luminosities of the Lyα and He II emission lines; references have been abbreviated to the first two letters of the first author's surname and the last two digits of the publication year, and the abbreviations are appended to the full bibliographic references at the end of this paper.

Source name	z	$S_{1.1}$ (mJy)	$L_{\text{Lyα}}$ (slit) (10^{44} erg s^{-1})	$L_{\text{Lyα}}$ (image) (10^{44} erg s^{-1})	Lyα/He II	$L_{\text{Lyα}}/L_{\text{FIR}}$	D_{radio} (kpc)	Refs
(1)	(2)	(3)	(4)	(5)	(6)	(7)	(8)	(9)
MRC 2201−555	0.51	6.1 ± 0.8	–	–	–	–	22	Bu06
MRC 2008−068	0.55	8.6 ± 0.9	–	–	–	–	0.2	Je00
MRC 2322−052	1.19	<2.0	–	–	–	–	64	Be99
TXS 2322−040	1.51	2.3 ± 0.6	–	–	–	–	0.5	Li07
MRC 2048−272	2.06	2.3 ± 0.8	–	0.65	–	0.0035	70	Pe00 Ve07
MRC 0355−037	2.15	5.0 ± 0.8	0.40	–	3.0	0.0010	101	Go05 Rö97
PKS 1138−262	2.16	<3.4	1.7	25	10.7	>0.025	80	Ca97 Rö97 Ve07
4C +23.56	2.48	<1.4	0.40	2.1	5.3	>0.018	390	Ca97 Ch96 Rö97 Ci98 Kn97
MRC 2104−242	2.49	3.7 ± 0.9	2.9	–	13	0.010	180	Pe00 Vi99 Ov01
PKS 0529−549	2.58	6.4 ± 0.7	0.41	–	12.3	0.00084	10	Br07 Rö97
MRC 0316−257	3.13	<1.9	0.21	0.7	–	>0.0047	59	Ca97 At98 Ve07
TN J2009−3040	3.16	3.3 ± 0.9	1.4	3.0	24.3	0.013	54	Bo07 DeBr00 Ve07
4C +41.17	3.79	3.5 ± 1.0	2.1	13	26.5	0.054	145	Ch90 Ch96 Rö97 Re03
TN J2007−1316	3.83	2.8 ± 0.9	0.26	–	9.0	0.0014	26	Bo07 DeBr00
TN J1338−1942	4.10	<4.7	1.7	4.5	18.4	>0.014	80	Pe00 DeBr99 DeBr01 Ve07
TN J0924−2201	5.19	3.6 ± 0.9	0.10	0.15	–	0.00074	8	vB99 DeBr01 Ve07

Table 4. Photometric measurements from the *Spitzer* observations of our sample of high-*z* active galaxies.

Source name	z	$S_{3.6}$ (μJy)	$S_{4.5}$ (μJy)	$S_{5.8}$ (μJy)	$S_{8.0}$ (μJy)	S_{24} (μJy)
MRC 2201−555	0.51	377 ± 6	401 ± 7	522 ± 22	640 ± 27	1547 ± 255
MRC 2322−052	1.19	147 ± 2	124 ± 2	96 ± 5	90 ± 5	–
TXS 2322−040	1.51	–	–	–	–	51 ± 15
MRC 2048−272	2.06	61 ± 2	71 ± 3	91 ± 14	73 ± 20	268 ± 61
MRC 0355−037	2.15	32 ± 1	35 ± 1	42 ± 4	48 ± 5	812 ± 136
PKS 1138−262	2.16	353 ± 5	522 ± 9	1048 ± 44	2024 ± 85	5111 ± 824
4C +23.56	2.48	60 ± 1	80 ± 1	164 ± 7	505 ± 21	5409 ± 876
MRC 2104−242	2.49	27 ± 6	33 ± 7	37 ± 22	<75	876 ± 255
PKS 0529−549	2.58	46 ± 2	55 ± 2	68 ± 12	102 ± 14	632 ± 110
MRC 0316−257	3.13	27.1 ± 0.5	27.2 ± 0.6	30 ± 2	57 ± 3	661 ± 118
TN J2009−3040	3.16	–	–	–	–	18 ± 4
4C +41.17	3.79	21.3 ± 0.6	26.0 ± 0.7	36 ± 3	52 ± 4	467 ± 82
TN J2007−1316	3.83	62 ± 2	61 ± 3	65 ± 14	172 ± 20	594 ± 102
TN J1338−1942	4.10	21.8 ± 0.8	12.8 ± 0.6	17 ± 3	17 ± 3	283 ± 61
TN J0924−2201	5.19	6.7 ± 0.3	10 ± 3	9.7 ± 0.9	<37	217 ± 68
SDSS J1030+0524	6.28	86 ± 1	109 ± 2	92 ± 5	109 ± 7	523 ± 92

At $z \gtrsim 2$, Lyα is redshifted into the optical regime, making this line accessible to ground-based telescopes. Indeed, all 11 of the $z \geq 2.15$ radio galaxies in our sample have measurements in the literature for the narrow (FWHM $\lesssim 3000$ km s^{-1}) Lyα emission. In Table 3, we list the Lyα luminosity for these 11 radio galaxies, determined for narrow-band images (e.g. Knopp & Chambers 1997; Reuland et al. 2003a; Venemans et al. 2007), and/or from spectra with a long-slit placed along the major axis of the radio emission (e.g. De Breuck et al. 2000a).

It is interesting to compare these obtained Lyα luminosities against the expected (intrinsic) Lyα luminosity of a massive star-burst. First, we derive an approximate relationship between the Lyα luminosity and SFR or L_{FIR}, as

$$L_{\text{Lyα}} \sim 10^{44}(\text{SFR}/100\,\text{M}_\odot\,\text{yr}^{-1})\,\text{erg s}^{-1}, \quad (6)$$

$$L_{\text{Lyα}} \sim 10^{44}(L_{\text{FIR}}/10^{12}\,\text{L}_\odot)\,\text{erg s}^{-1}, \quad (7)$$

which simplifies to become

$$L_{\text{Lyα}}/L_{\text{FIR}} \sim 0.03 \quad (8)$$

under the assumptions that (i) the starburst is continuous and has an age in the range of ~1–5 Myr; (ii) all ionizing photons produced
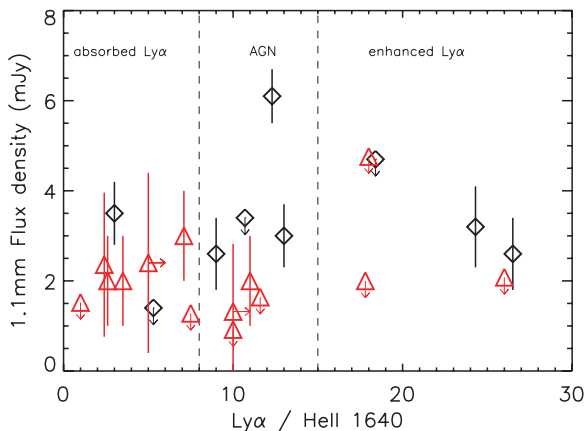
Figure 7. Flux density at 1.1 mm versus Lyα/He II. Dashed vertical lines separate three different areas on the plot: Lyα/He II lower than predicted by AGN photoionization models (absorbed); Lyα/He II consistent with AGN photoionization models; and Lyα/He II higher than predicted by AGN photoionization models (enhanced). Black diamonds show the high-z radio galaxies from our sample which have Lyα/He II measurements in the literature. Red triangles show high-z radio galaxies from the literature which have both SCUBA 850 μm flux density measurements, which we have scaled by a factor of 0.4 to account for the shorter wavelength, and Lyα/He II measurements, the latter from Villar-Martín et al. (2007).

by the stars are absorbed in the surrounding H II region; and (iii) 67 per cent of photoionization events lead to the emission of a Lyα photon (Binette et al. 1993). Of the eight galaxies in our sample which have been detected both in Lyα emission and in 1.1-mm continuum emission, three have values of $L_{Lyα}/L_{FIR}$ which are in an order-of-magnitude agreement with the expected value ∼0.03, and five have $L_{Lyα}/L_{FIR}$ values more than an order of magnitude lower (Table 3).

Thus far, we have ignored another luminous source of ionizing radiation which is likely to contribute significantly to the production of Lyα photons – the active nucleus. The ratio between Lyα and He II λ1640 is sensitive to the SED of the ionizing continuum and, therefore, it can be used to assess the extent to which stellar-photoionized H II regions contribute to the UV–optical emission line spectrum. Models for pure AGN photoionization predict Lyα/He II = 8–15 (e.g. Humphrey et al. 2008), depending on the spectral slope of the ionizing continuum between 13.6 and 54.4 eV. On the other hand, photoionization by young stars does not result in significant He II emission relative to Lyα. Thus, a Lyα/He II ratio significantly in excess of 15 would suggest a significant contribution from stellar-photoionized H II regions. A number of HzRGs, including three of our sample (TN J2009−3040, 4C+41.17 and TN J1338−1942), do indeed show such an excess of Lyα emission. Villar-Martín et al. (2007) examined the Lyα/He II and Lyα/CIV ratios of 61 radio galaxies at $1.79 \le z \le 4.41$, and identified a Lyα excess in 11 of their sample; they calculated that an SFR of ∼200 $M_{\odot}$ yr^{-1} would be required to explain the most extreme objects.

Naively, one might expect there to be a correlation between detection of a Lyα excess and detection of millimetre continuum, since both are thought to be produced by powerful starbursts. In Fig. 7 we plot $S_{1.1}$ against the Lyα/He II ratio for radio galaxies from our sample which have Lyα and He II detections. We also plot radio galaxies which have been observed at 850 μm (from table 1 of Villar-Martín et al. 2007), under the assumption that $S_{1.1} = S_{850}/2.5$. Contrary to initial expectations, we find no trend between $S_{1.1}$ and Lyα/He II. The possible origin of this result is discussed in Section 6.
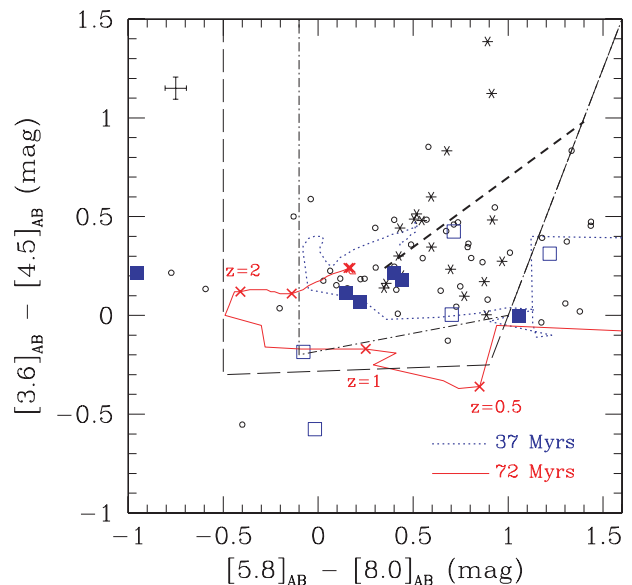

Figure 8. *Spitzer* IRAC [3.6]–[4.5] versus [5.8]–[8.0] colour–colour diagram for the radio galaxies in our sample which have been detected in all the four bands (adapted from Stern et al. 2005). Solid squares are HzRGs for which we have detected a probable 1.1-mm counterpart; open squares are HzRGs for which we have not detected a probable 1.1-mm counterpart. The small open circles are the HzRG sample of Seymour et al. (2007). Asterisks (∗) show the infrared quasars with power-law spectra from Lacy et al. (2004) and Martínez-Sansigre et al. (2008). The dot–dashed line indicates the AGN region proposed by Stern et al. (2005). The long-dashed black line shows the MMG counterpart region proposed by Yun et al. (2008). The dotted line and the solid line show the redshift evolution colour–colour track for a starburst age of 37 and 72 Myr, respectively, based on the theoretical starburst spectral energy distribution models of Efstathiou, Rowan-Robinson & Siebenmorgan (2000); crosses (x) along the 72-Myr track mark z = 0.5, 1, 2, 3, 4 and 5. The thick short-dashed line represents power-law spectrum sources having $α = 0.3$–1.0, where $S_v \propto v^{-α}$.

5 ANALYSIS OF THE MID-IR SPECTRAL ENERGY DISTRIBUTION

In Fig. 8 we show the *Spitzer* IRAC [3.6]–[4.5] versus [5.8–8.0] colour diagram, adapted from Stern et al. (2005), for all HzRGs in our sample that are detected in all the four IRAC channels (Table 4). Most of our target HzRGs as well as those studied by Seymour et al. (2007) are found within the region of red rest-frame optical and near-IR colour characteristic of hot dust, overlapping with the distribution of the *Spitzer*-selected power-law quasars of Lacy et al. (2004) and Martínez-Sansigre et al. (2008). While the colours of our target HzRGs are marginally consistent with colours expected of active galaxies, those detected by AzTEC (filled squares) appear near the edges of the distribution, along the model tracks of young dust-obscured stellar clusters modelled by Efstathiou et al. (2000). This is also the area where the majority of submillimetre-bright sources are clustered (Yun et al. 2008, 2011), and these AzTEC-detected HzRGs display rest-frame near-IR properties more like SMGs than other HzRGs.

The diagram shown in Fig. 9 aims to distinguish active galaxies from starburst systems using two different diagnostic criteria proposed recently by different groups: (1) $S_{24}/S_R > 1000$ (dark optical galaxies, or DOGs: Dey et al. 2008; Fiore et al. 2008); and (2) $S_{8.0}/S_{4.5} > 2$ (Ivison et al. 2004; Pope et al. 2008). The DOGs were first identified in the study of a population of $z \sim 2$ infrared bright galaxies that are extremely faint in the optical bands, and Fiore et al.
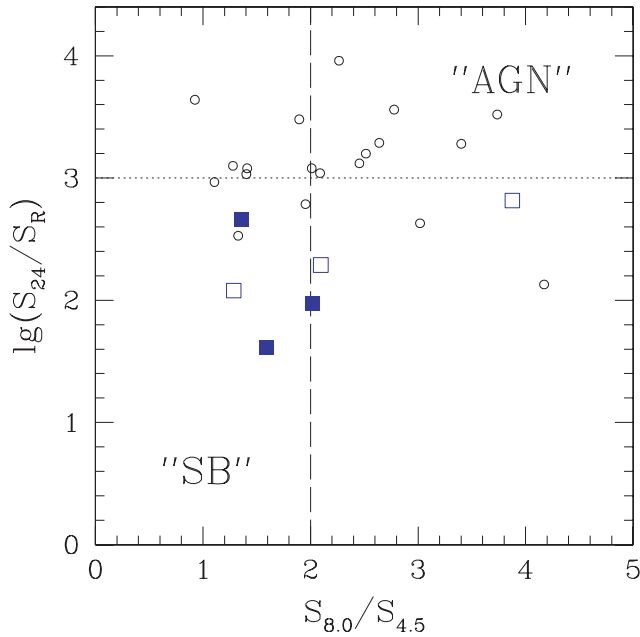
Figure 9. Log S_{24}/S_R versus $S_{8.0}/S_{4.5}$ for the radio galaxies in our sample which have been detected in the *Spitzer* MIPS 24-μm channel, in the IRAC 4.5- and 8.0-μm channels, and in the optical R band. Filled squares show radio galaxies for which we have detected a probable counterpart at 1.1 mm; open squares show radio galaxies for which we have not detected a probably 1.1-mm counterpart. The small circles are the HzRG sample of Seymour et al. (2007) as in Fig. 8. Note that S_R is the flux density corresponding to the R or r magnitude of the radio galaxy. References to the optical photometry are as follows: MRC 2201−555, Bu06; MRC 0355−037, Go05; PKS 1138−262, Pe97; MRC 0316−257, Mc96; 4C +41.17, Mi92; TN J1338−1942, DeBr02. Starburst galaxies (SB) are expected to lie at Log $S_{24}/S_R < 3$, $S_{8.0}/S_{4.5} < 2$, whereas active galaxies are expected to lie above and/or to the right of this region of colour space (see Dey et al. 2008; Fiore et al. 2008; Pope et al. 2008).

(2008) concluded based on their X-ray analysis that as many as 80 per cent of these dust-obscured galaxies host a Compton-thick AGN. The latter criterion was initially developed to exploit the presence of polycyclic aromatic hydrocarbon (PAH) features and a power-law AGN spectral shape in the rest-frame near-IR, similar to the information used in Fig. 8.

In this diagram, the majority of the HzRGs detected in MIPS 24 μm by Seymour et al. (2007) appear above the DOGs line of $S_{24}/S_R > 1000$ (dotted line), suggesting that warm dust and a heavily obscured AGN are present in these HzRGs. All six of our target HzRGs detected in the MIPS 24-μm bands are below the dotted line and are on average bluer than the others. In fact, the three AzTEC-detected HzRGs are among the bluest HzRGs. The AzTEC-detected HzRGs also show a flatter $S_{8.0}/S_{4.5}$ flux ratio than the rest of the HzRGs. Taken together, these rest-frame optical and near- and mid-IR diagnostic colours suggest that the AzTEC-detected HzRGs have bluer colours of star-forming galaxies than those of dust-obscured AGNs with characteristic hot dust emission commonly associated with other HzRGs. We note that the overall rest-frame optical colours of even the most dusty star-forming galaxies, such as ultraluminous infrared galaxies in the local Universe, are surprisingly blue because young stellar populations distributed throughout the galaxy dominate the overall colour and luminosity (see Chen, Lowenthal & Yun 2010).

In summary, HzRGs that have an AzTEC counterpart also have mid-infrared spectral energy distributions that are consistent with dust-obscured starburst systems.

5.1 24-μm images

In Fig. 10 we show 160×160 arcsec^2 postage stamps of the 24-μm emission, with contours of the 1.1-mm emission overlayed, in order to illustrate interesting morphological features around three of the radio galaxies. A detailed analysis of clustering in the full 170–300 arcmin^2 fields (as opposed to the 7 arcmin^2 'postage stamps' considered herein) of our sample of 17 high-z active galaxies will be presented in a future paper (Zeballos et al., in preparation).

5.1.1 MRC 2201−555

The 24 μm MIPS image shows an arc of emission running through the position of the radio galaxy, with a total spatial extent of ∼38 arcsec or 230 kpc. The north-west portion of the arc takes the form of a relatively bright source ∼16 arcsec (100 kpc) to the north-west, which is linked to the radio galaxy by a bridge of lower surface brightness emission. This structure is too compact to resolve at the resolution of our AzTEC/ASTE observation.

5.1.2 MRC 0355−037

The MIPS image shows an arc comprised of several 24-μm sources extending ∼60 arcsec (∼500 kpc) to the west-south-west from the position of the radio galaxy. At or near the end of this arc, our AzTEC map shows a peak that has S/N = 2.6, after correcting for the negative sidelobes of the radio galaxy's AzTEC counterpart.

5.1.3 TN J2007−1318

An arc of several 24-μm sources extends ∼50 arcsec (∼360 kpc) SSE from the radio galaxy. Similarly, in our AzTEC image there is an arc of 1.1-mm emission, cospatial with the 24-μm arc, with peak S/N = 2.4 after correcting for the negative sidelobes of radio galaxy's 1.1-mm counterpart.

6 DISCUSSION

In the process of this study, we have identified a statistically significant anticorrelation between the size of the radio source and the brightness of the millimetre continuum emission (or SFR). This is by no means the first investigation into the possible relationships between the size of a radio source and the other properties of radio galaxies; numerous relationships have been found previously between the observed size of powerful radio sources and various UV, optical and infrared properties. Best et al. (1996) found a morphological evolution with radio size in their sample of eight 3CR radio galaxies at $1 < z < 1.3$. For galaxies with relatively smaller radio sources, their *HST* images reveal a string of bright knots tightly aligned with the radio emission. The galaxies with relatively larger radio sources, while still showing the alignment effect (e.g. Chambers et al. 1987; McCarthy et al. 1987), are generally more compact and contain fewer bright optical knots. Furthermore, in galaxies with smaller radio sources, the extended emission line region (EELR) tends to have a relatively smaller observed spatial extent, as measured with Lyα (van Ojik et al. 1997). The EELR of these galaxies also show more extreme emission line kinematics, have brighter UV–optical emission lines, and ratios between emission lines that imply that they have lower ionization states
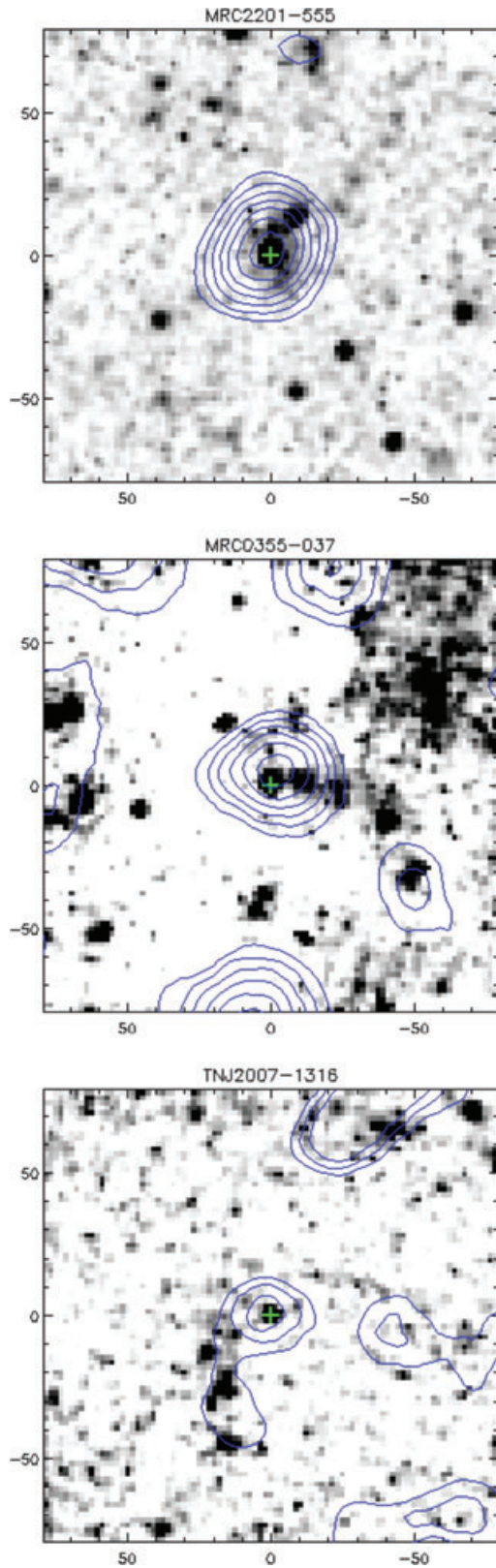
Figure 10. Postage stamps of the 24-μm emission (grey-scale) with contours of the 1.1-mm emission overlayed. For MRC 2201−555, the AzTEC contours are the same as in Fig. 1. For MRC 0355−037, the contours start at 1σ and increase by 1σ. For TN J2007−1316, the contours are 1.7σ, 2.2σ, 2.7σ. North and east are at the top and left of the images, respectively. The cross (+) marks the position of the active galaxy.
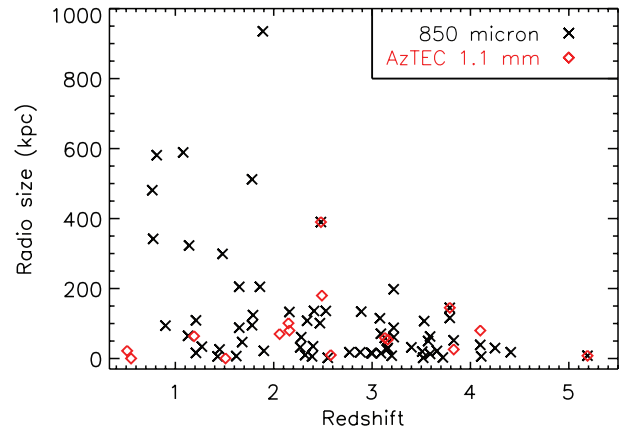

Figure 11. Radio size as a function of *z*. In the interest of clarity, error bars are not shown. Note the clear anticorrelation between these two parameters, which complicates interpretation of any observed evolution of properties with *z* (see text).

(Best et al. 2000; Inskip et al. 2002; Humphrey et al. 2006). In addition, the polarization of the rest-frame UV continuum emission is correlated with radio source size (Solórzano-Iñarrea et al. 2004), suggesting that the ratio between scattered light and starlight is relatively higher in radio galaxies with larger radio sources. The anticorrelation between 850-μm luminosity and UV continuum polarization found by Reuland et al. (2004) appears to confirm that the UV continuum polarization is indeed strongly dependent on the rate of star formation. Furthermore, HzRGs showing anomalously high values of Lyα/He II ($\gtrsim 15$), likely due to the presence of a powerful starburst (~ 100 $M_\odot$ yr^{-1}), tend to have smaller radio sources than those with 'normal' or 'low' values (Villar-Martín et al. 2007). These radio-optical trends are commonly supposed to be the result of (a) interaction between the radio source and the host galaxy, (b) slowing of radio source expansion in radio galaxies that are in relatively denser environments, or (c) age effects of the radio source.

A previously unanswered question was whether the SFR is intrinsically higher in HzRGs with smaller radio sources, or whether instead the UV–optically derived SFR merely appears higher due to some difference in dustiness, geometry, etc. Observations in the millimetre/submillimetre regime give us a new perspective from which we may address this question, since the observations are sensitive to UV–optically obscured (rather than unobscured) star-forming regions. Assuming that the millimetre/submillimetre continuum is dominated by thermal emission from starburst-heated dust, as we believe to be the case, then our anticorrelation between $S_{1.1}$ and radio size leads us to conclude that HzRGs with relatively smaller radio sources do indeed tend to have intrinsically higher SFR.

In light of this conclusion, it seems natural to now question whether the increase in the millimetre/submillimetre detectability of HzRGs at $z \geq 2.5$ is due to a genuine redshift evolution in the rate or mode of star formation in the host galaxies, as has commonly been supposed (Archibald et al. 2001; Reuland et al. 2004). Indeed, we propose an alternative hypothesis: that there is a bias towards identifying HzRGs with smaller radio sources at higher *z* (Fig. 11) because these sources are associated with more luminous narrow emission line regions (e.g. Best et al. 2000). And since smaller radio sources typically have more luminous millimetre/submillimetre emission (Figs 5 and 6), we propose that this translates into a bias in favour of identifying HzRGs with significantly more luminous millimetre/submillimetre emission at higher *z*. Identifying and studying the 'missing', line-weak HzRGs will be crucial for testing this

hypothesis (see Reuland et al. 2003b; Reuland 2005; Miley & De Breuck 2008).

It is not known whether the observed size of the radio source is determined primarily by the density of the interstellar/intergalactic medium through which the source propagates, or whether the size is instead determined primarily by the age of the radio source. If we were to assume the latter, then we would be able to gauge the lifetime of luminous, dusty star formation episodes ($S_{1.1} > 2.5$ mJy; SFR $> 500\,M_{\odot}\,\mathrm{yr}^{-1}$) closely associated with HzRGs. In Fig. 5, all of the luminous millimetre counterparts are associated with HzRGs that have radio source diameters of $d < 200$ kpc: we adopt $d \sim 200$ kpc as the approximate stage in the growth of the radio source at which the luminous millimetre counterparts fade to $S_{1.1} < 2.5$ mJy (SFR $< 500\,M_{\odot}\,\mathrm{yr}^{-1}$). Assuming a conservative expansion speed of $\sim 0.01c$ for the radio source (e.g. Best et al. 1995), this diameter implies an age of ~ 30 Myr. A similar age was estimated by Willott et al. (2002) for a smaller sample of high-z, radio-loud quasars. However, we must be cautious about generalizing this to obscured star formation in non-active galaxies (i.e. to submillimetre galaxies in general): HzRGs contain two powerful sources of feedback, the radio source and the accretion disc, both of which are able to quench star formation and, perhaps, to ignite it. Conceivably, feedback of this kind could either lengthen or shorten the lifetimes of star formation activity in HzRGs, and could mean that lifetimes of obscured star formation activity determined for HzRGs are not necessarily representative of those for millimetre/submillimetre galaxies in general.

We have also investigated whether there might be a correlation between the millimetre flux density and the Lyα/He II ratio, which is expected to be sensitive to SFR also. While Lyα can originate from stellar photoionized H II regions and from AGN-ionized nebulae, the He II line is expected to come predominantly from nebulae that are ionized by the AGN. Though both Lyα/He II and the millimetre flux density are expected to be correlated with SFR, and therefore with each other, no significant trend was found between them. Furthermore, the luminosity of the Lyα emission is often more than an order of magnitude lower than one would have expected given the SFR derived from the 1.1-mm flux density (we estimate $L_{\mathrm{Ly}\alpha}/L_{\mathrm{FIR}} \sim 0.0007$–$0.054$, while the expected value is ~ 0.03). This may mean that one (or both) of the millimetre and Lyα emission is an inaccurate tracer of the SFR in HzRGs. This could be due to destruction of Lyα photons by the dust associated with this kind of star formation activity.

Thus far, we have tacitly assumed that the sources we identify as 1.1-mm counterparts are the radio galaxy hosts themselves. However, it is important to be aware that the spatial resolution of our observations, together with the signal-to-noise ratios of the detections, has resulted in 1σ positional uncertainties of ~ 2–16 arcsec for our 1.1-mm counterparts. This means that the sources we identify as 1.1-mm counterparts could in fact be offset by tens or even hundreds of kpc from the galactic nucleus, which would place them on the outskirts or outside of the host galaxy. This may be the case for TN J0924$-$2201, which is undetected in SCUBA photometry (Reuland et al. 2004), but which according to our criteria has a 1.1-mm counterpart in our AzTEC map (Section 3.2) – this suggests that the AzTEC source is not the actual counterpart, but is instead an MMG several tens of kpc from the radio galaxy. Also of relevance in this context are results from an FWHM = 2 arcsec spatial resolution submillimeter array study of the $z = 3.79$ radio galaxy 4C +60.07 (Ivison et al. 2008): the luminous submillimetre emission, previously assumed to be centred on the active galaxy's host, was resolved into two discrete submillimetre sources with offsets of 1 arcsec (~ 10 kpc) and 4 arcsec (~ 30 kpc) from the position of the radio core. These two results provide evidence, although anecdotal in nature, that the millimetre/submillimetre emission associated with high-z radio galaxies may not always be spatially coincident with the host galaxy. Unfortunately, with currently available facilities high-resolution observations of the kind presented by Ivison et al. (2008) are costly and are sensitive only to the very brightest of MMGs. The next generation of millimetre/submillimetre facilities, such as the 50-m Large Millimetre Telescope or the Atacama Large Millimetre Array, will be needed to resolve this issue.

Nevertheless, we can state that all 17 of the active galaxies in our sample are associated with one or more MMG, and thus we conclude that high-z (radio-loud) active galaxies are beacons for finding MMGs.

7 SUMMARY

We have presented 1.1-mm imaging observations of the 7 arcmin^2 fields around 16 powerful radio galaxies at $0.5 < z < 5.2$ and a radio-quiet quasar at $z = 6.3$. With these new observations, we have more than doubled the number of high-z radio galaxies which have been imaged at millimetre/submillimetre wavelengths. For all 17 active galaxies, we detect at least one associated millimetric source, which shows that high-z (radio-loud) active galaxies are beacons for finding millimetre/submillimetre galaxies at high-z. We identify likely millimetric counterparts for 11 radio galaxies, and these have 1.1-mm flux densities ranging between <1.4 mJy (3σ) and 8.6 ± 0.9 mJy, with implied SFRs of <200 to $\sim 1300\,M_{\odot}\,\mathrm{yr}^{-1}$. After stacking our images at the position of the radio galaxies, including those for which we did not detect the millimetric counterpart, we derive an average flux density of 3.4 ± 0.2 mJy.

For the high-z radio galaxies, we have identified an anticorrelation between 1.1-mm flux density (or SFR) and the projected linear size of the radio source. From this result, we have concluded that smaller radio sources are associated with more powerful (obscured) starbursts.

We have also presented images and photometry from new and archival *Spitzer* IRAC and MIPS observations. We find that the mid-infrared spectral energy distributions of the radio galaxies tend to be bluer than those of *Spitzer*-selected high-z active galaxies (Lacy et al. 2004; Martínez-Sansigre et al. 2008). In particular, the radio galaxies which we have detected at 1.1 mm have mid-infrared colours consistent with obscured star formation. We have also identified three ≥ 100 kpc arcs of 24-μm sources of which three radio galaxies appear to be parts; for the two arcs at $z > 2$, we note a spatial correlation between the 24- and 1.1-mm emissions.

the Netherlands Organisation for Scientific Research, and the National Research Council of Canada. The ASTE project is driven by the Nobeyama Radio Observatory (NRO), a branch of the National Astronomical Observatory of Japan (NAOJ), in collaboration with the University of Chile and Japanese institutions including the University of Tokyo, Nagoya University, Osaka Prefecture University, Ibaraki University and Hokkaido University.

REFERENCES

Archibald E. N., Dunlop J. S., Hughes D. H., Rawlings S., Eales S. A., Ivison R. J., 2001, MNRAS, 323, 417

Athreya R. M., Kapahi V. K., McCarthy P. J., van Breugel W., 1998, A&A, 329, 809 (At98)

Austermann J. E. et al., 2010, MNRAS, 401, 160

Becker R. H., White R. L., Edwards A. L., 1991, ApJS, 75, 1 (Be91)

Benford D. J., 1999, PhD thesis, California Instit. Technol. (Be99)

Bertin E., Arnouts S., 1996, A&AS, 117, 393

Best P. N., Bailer D. M., Longair M. S., Riley J. M., 1995, MNRAS, 275, 1171

Best P. N., Longair M. S., Röttgering H. J. A., 1996, MNRAS, 280, L9

Best P. N., Röttgering H. J. A., Lehnert M. D., 1999, MNRAS, 310, 223 (Be99)

Best P. N., Röttgering H. J. A., Longair M. S., 2000, MNRAS, 311, 23

Binette L., Wang J., Villar-Martin M., Martin P. G., Magris C. G., 1993, ApJ, 414, 535

Black A. R. S., Baum S. A., Leahy J. P., Perley R. A., Riley J. M., Scheuer P. A. G., 1992, MNRAS, 256, 186

Blundell K. M., 1996, MNRAS, 283, 538

Bolton J. G., Shimmins A. J., Wall J. V., 1975, Australian J. Phys. A, 34, 1 (Bo75)

Bornancini C. G., De Breuck C., de Vries W., Croft S., van Breugel W., Röttgering H., Minniti D., 2007, MNRAS, 378, 551 (Bo07)

Broderick J. W., De Breuck C., Hunstead R. W., Seymour N., 2007, MNRAS, 375, 1059 (Br07)

Burgess A. M., Hunstead R. W., 2006, AJ, 131, 114 (Bu06)

Carilli C. L., Roettgering H. J. A., van Ojik R., Miley G. K., van Breugel W. J. M., 1997, ApJS, 109, 1 (Ca97)

Carilli C. L., Wang R., van Hoven M. B., Dwarakanath K., Chengalur J. N., Wyithe S., 2007, AJ, 133, 2841 (Ca07)

Chambers K. C., Miley G. K., van Breugel W., 1987, Nat, 329, 604

Chambers K. C., Miley G. K., van Breugel W. J. M., 1990, ApJ, 363, 21 (Ch90)

Chambers K. C., Miley G. K., van Breugel W. J. M., Bremer M. A. R., Huang J.-S., Trentham N. A., 1996, ApJS, 106, 247 (Ch96)

Chen Y., Lowenthal J. D., Yun M. S., 2010, ApJ, 712, 1385

Chini R., Krügel E., Kreysa E., 1986, A&A, 167, 315

Cimatti A., di Serego Alighieri S., Vernet J., Cohen M., Fosbury R. A. E., 1998, ApJ, 499, L21 (Ci98)

Cohen A. S., Lane W. M., Cotton W. D., Kassim N. E., Lazio T. J. W., Perley R. A., Condon J. J., Erickson W. C., 2007, AJ, 134, 1245 (Co07)

Condon J. J., Cotton W. D., Greisen E. W., Yin Q. F., Perley R. A., Taylor G. B., Broderick J. J., 1998, AJ, 115, 1693 (Co98)

De Breuck C., van Breugel W., Minniti D., Miley G., Röttgering H., Stanford S. A., Carilli C., 1999, A&A, 352, L51 (DeBr99)

De Breuck C., Röttgering H., Miley G., van Breugel W., Best P., 2000a, A&A, 362, 519

De Breuck C., van Breugel W., Röttgering H. J. A., Miley G., 2000b, A&AS, 143, 303 (DeBr00)

De Breuck C. et al., 2001, AJ, 121, 1241 (DeBr01)

De Breuck C., van Breugel W., Stanford S. A., Röttgering H., Miley G., Stern D., 2002, AJ, 123, 637 (DeBr02)

De Breuck C. et al., 2004, A&A, 424, 1 (DeBr04)

De Breuck C. et al., 2010, ApJ, 725, 36

Dey A. et al., 2008, ApJ, 677, 943

Douglas J. N., Bash F. N., Bozyan F. A., Torrence G. W., Wolfe C., 1996, AJ, 111, 1945 (Do96)

Downes A. J. B., Peacock J. A., Savage A., Carrie D. R., 1986, MNRAS, 218, 31

Downes D., Solomon P. M., Sanders D. B., Evans A. S., 1996, A&A, 313, 91

Downes T. P., Welch D. E., Scott K., Austermann J., Wilson G. W., 2011, preprint (arXiv:1103.3072)

Dunlop J. S., Hughes D. H., Rawlings S., Eales S. A., Ward M. J., 1994, Nat, 370, 347

Dunlop J., Peacock J., Spinrad H., Dey A., Jimenez R., Stern D., Windhorst R., 1996, Nat, 381, 581

Efstathiou A., Rowan-Robinson M., Siebenmorgan R., 2000, MNRAS, 313, 734

Ezawa H., Kawabe R., Kohno K., Yamamoto S., 2004, in Oschmann J. M., Jr, ed., Proc. SPIE Vol. 5489, Ground-based Telescopes. SPIE, Bellingham, 763E

Fan X. et al., 2001, AJ, 122, 2833

Fanti C., Fanti R., Ficarra A., Padrielli L., 1974, A&AS, 18, 147 (Fa74)

Fazio G. G. et al., 2004, ApJS, 154, 10

Ficarra A., Grueff G., Tomassetti G., 1985, A&AS, 59, 255 (Fi85)

Fiore F. et al., 2008, ApJ, 672, 94

Foley R. J., 2011, ApJ, 731, 86

Gopal-Krishna, Ledoux C., Melnick J., Giraud E., Kulkarni V., Altieri B., 2005, A&A, 436, 457 (Go05)

Gower J. F. R., Scott P. F., Wills D., 1967, Mem. R. Astron. Soc., 71, 49 (Go67)

Gregory P. C., Condon J. J., 1991, ApJS, 75, 1011 (Gr91)

Gregory P. C., Vavasour J. D., Scott W. K., Condon J. J., 1994, ApJS, 90, 173 (Gr94)

Greve T. R., Stern D., Ivison R. J., De Breuck C., Kovács A., Bertoldi F., 2007, MNRAS, 382, 48 (Gr07)

Griffith M., Langston G., Heflin M., Conner S., Lehar J., Burke B., 1990, ApJS, 74, 129 (Gr90)

Griffith M. R., Wright A. E., Burke B. F., Ekers R. D., 1994, ApJS, 90, 179 (Gr94)

Griffith M. R., Wright A. E., Burke B. F., Ekers R. D., 1995, ApJS, 97, 347 (Gr95)

Gutermuth R. A., Myers P. C., Megeath S. T., Allen L. E., Pipher J. L., Muzerolle J., Porras A., Winston E., Fazio G., 2008, ApJ, 674, 336

Hales S. E. G., Baldwin J. E., Warner P. J., 1993, MNRAS, 263, 25 (Ha93)

Hatch N. A., Overzier R. A., Kurk J. D., Miley G. K., Röttgering H. J. A., Zirm A. W., 2009, MNRAS, 395, 114

Healey S. E., Romani R. W., Taylor G. B., Sadler E. M., Ricci R., Murphy T., Ulvestad J. S., Winn J. N., 2007, ApJS, 171, 61 (He07)

High F. W. et al., 2010, ApJ, 723, 1736

Hildebrand R. H., 1983, QJRAS, 24, 267

Humphrey A., Villar-Martín M., Fosbury R., Vernet J., di Serego Alighieri S., 2006, MNRAS, 369, 1103

Humphrey A., Villar-Martín M., Fosbury R., Binette L., Vernet J., De Breuck C., di Serego Alighieri S., 2007, MNRAS, 375, 705

Humphrey A., Villar-Martín M., Vernet J., Fosbury R., di Serego Alighieri S., Binette L., 2008, MNRAS, 383, 11

Inskip K. J., Best P. N., Röttgering H. J. A., Rawlings S., Cotter G., Longair M. S., 2002, MNRAS, 337, 1407

Isobe T., Feigelson E. D., Nelson P. I., 1986, ApJ, 306, 490

Ivison R. J., Dunlop J. S., Smail Ian, Dey Arjun, Liu Michael C., Graham J. R., 2000, ApJ, 542, 27

Ivison R. J. et al., 2004, ApJS, 154, 124

Ivison R. J. et al., 2007, MNRAS, 380, 199

Ivison R. J. et al., 2008, MNRAS, 390, 1117

Jeyakumar S., Saikia D. J., Pramesh Rao A., Balasubramanian V., 2000, A&A, 362, 27 (Je00)

Kim S. et al., 2009, ApJ, 695, 809

Knopp G. P., Chambers K. C., 1997, ApJS, 109, 367 (Kn97)

Kuehr H., Witzel A., Pauliny-Toth I. I. K., Nauber U., 1981, A&AS, 45, 367 (Ku81)

Lacy M. et al., 2004, ApJS, 154, 166

Large M. I., Mills B. Y., Little A. G., Crawford D. F., Sutton J. M., 1981, MNRAS, 194, 693 (La81)

Liu X., Cui L., Luo W.-F., Shi W.-Z., Song H.-G., 2007, A&A, 470, 97 (Li07)

Martínez-Sansigre A., Lacy M., Sajina A., Rawlings S., 2008, ApJ, 674, 676

Mauch T., Murphy T., Buttery H. J., Curran J., Hunstead R. W., Piestrzynski B., Robertson J. G., Sadler E. M., 2003, MNRAS, 342, 1117 (Ma03)

McCarthy P. J., van Breugel W., Spinrad H., Djorgovski S., 1987, ApJ, 321, L29

McCarthy P. J., Spinrad H., van Breugel W., 1995, ApJS, 99, 27

McCarthy P. J., Kapahi V. K., van Breugel W., Persson S. E., Athreya R., Subrahmanya C. R., 1996, ApJS, 107, 19 (Mc96)

McLure R. J., Kukula M. J., Dunlop J. S., Baum S. A., O'Dea C. P., Hughes D. H., 1999, MNRAS, 308, 377

Menanteau F. et al., 2010, ApJ, 723, 1523

Miley G., De Breuck C., 2008, A&AR, 15, 67

Miley G. K., Chambers K. C., van Breugel W. J. M., Macchetto F., 1992, ApJ, 401, L69 (Mi92)

Murgia M., Fanti C., Fanti R., Gregorini L., Klein U., Mack K.-H., Vigotti M., 1999, A&A, 345, 769

Muxlow T. W. B., Pelletier G., Roland J., 1988, A&A, 206, 237

Nesvadba N. P. H. et al., 2006, ApJ, 650, 661

Nesvadba N. P. H. et al., 2009, MNRAS, 395, L16

Overzier R. A., Röttgering H. J. A., Kurk J. D., De Breuck C., 2001, A&A, 367, L5 (Ov01)

Pentericci L., Roettgering H. J. A., Miley G. K., Carilli C. L., McCarthy P., 1997, A&A, 326, 580 (Pe97)

Pentericci L., Van Reeven W., Carilli C. L., Röttgering H. J. A., Miley G. K., 2000, A&AS, 145, 121 (Pe00)

Pentericci L., McCarthy P. J., Röttgering H. J. A., Miley G. K., van Breugel W. J. M., Fosbury R., 2001, ApJS, 135, 63

Pérez-Torres M.-A., De Breuck C., 2005, MNRAS, 363, 41

Pilkington J. D. H., Scott P. F., 1965, Mem. R. Astron. Soc., 69, 183 (Pi65)

Pope A. et al., 2008, ApJ, 689, 127

Priddey R. S., Isaak K. G., McMahon R. G., Robson E. I., Pearson C. P., 2003, MNRAS, 344, L74

Priddey R. S., Ivison R. J., Isaak K. G., 2008, MNRAS, 383, 289

Reuland M., 2005, PhD thesis, Leiden Obser., Leiden Univ.

Reuland M. et al., 2003a, ApJ, 592, 755 (Re03)

Reuland M., van Breugel W., Röttgering H., de Vries W., De Breuck C., Stern D., 2003b, ApJ, 582L, 71

Reuland M., Röttgering H., van Breugel W., De Breuck C., 2004, MNRAS, 353, 377 (Re04)

Ricci R., Prandoni I., Gruppioni C., Sault R. J., de Zotti G., 2006, A&A, 445, 465 (Ri06b)

Rickett B. J., Lazio T. J. W., Ghigo F. D., 2006, ApJS, 165, 439 (Ri06a)

Rieke G. H. et al., 2004, ApJS, 154, 25

Röttgering H. J. A., van Ojik R., Miley G. K., Chambers K. C., van Breugel W. J. M., de Koff S., 1997, A&A, 326, 505 (Rö97)

Scott K. et al., 2008, MNRAS, 385, 2225

Scott K. S. et al., 2010, MNRAS, 405, 2260

Seymour N. et al., 2007, ApJS, 171, 353

Slee O. B., 1995, Australian J. Phys., 48, 143 (Sl95)

Solórzano Iñarrea C., Best P. N., Röttgering H. J. A., Cimatti A., 2004, MNRAS, 351, 997

Stanghellini C., O'Dea C. P., Dallacasa D., Baum S. A., Fanti R., Fanti C., 1998, A&AS, 131, 303 (St98)

Stanghellini C., O'Dea C. P., Dallacasa D., Cassaro P., Baum S. A., Fanti R., Fanti C., 2005, A&A, 443, 891 (St05)

Stern D. et al., 2005, ApJ, 631, 163

Stevens J. A. et al., 2003, Nat, 425, 264

Stevens J. A., Jarvis M. J., Coppin K. E. K., Page M. J., Greve T. R., Carrera F. J., Ivison R. J., 2010, MNRAS, 405, 2623

Stiavelli M. et al., 2005, ApJ, 622, L1

van Breugel W., Miley G., Heckman T., Butcher H., Bridle A., 1985, ApJ, 290, 496

van Breugel W., De Breuck C., Stanford S. A., Stern D., Röttgering H., Miley G., 1999, ApJ, 518, L61 (vB99)

van Ojik R., Roettgering H. J. A., Miley G. K., Hunstead R. W., 1997, A&A, 317, 358

Venemans B. P. et al., 2007, A&A, 461, 823 (Ve07)

Vernet J., Fosbury R. A. E., Villar-Martín M., Cohen M. H., Cimatti A., di Serego Alighieri S., Goodrich R. W., 2001, A&A, 366, 7

Vieira J. D. et al., 2010, ApJ, 719, 763

Villar-Martín M., Fosbury R. A. E., Binette L., Tadhunter C. N., Rocca-Volmerange B., 1999, A&A, 351, 47 (Vi99)

Villar-Martín M., Vernet J., di Serego Alighieri S., Fosbury R., Humphrey A., Pentericci L., 2003, MNRAS, 346, 273

Villar-Martín M. et al., 2006, MNRAS, 366, L1

Villar-Martín M., Humphrey A., De Breuck C., Fosbury R., Binette L., Vernet J., 2007, MNRAS, 375, 1299

Viner M. R., Erickson W. C., 1975, AJ, 80, 931 (Vi75)

Werner M. W. et al., 2004, ApJS, 154, 1

White R. L., Becker R. H., 1992, ApJS, 79, 331 (Wh92)

Willott C. J., Rawlings S., Archibald E. N., Dunlop J. S., 2002, MNRAS, 331, 435

Willott C. J., Delfosse X., Forveille T., Delorme P., Gwyn S. D. J., 2005, ApJ, 633, 630

Wilson G. W. et al., 2008, MNRAS, 386, 807

Wright A., Otrupcek R., 1990, Parkes Catalogue, Australia Telescope National Facility (Wr90)

Wright A. E., Griffith M. R., Burke B. F., Ekers R. D., 1994, ApJS, 91, 111 (Wr94)

Xiang L., Dallacasa D., Cassaro P., Jiang D., Reynolds C., 2005, A&A, 434, 123 (Xi05)

Xiang L., Reynolds C., Strom R. G., Dallacasa D., 2006, A&A, 454, 729 (Xi06)

Yun M. S. et al., 2008, MNRAS, 389, 333

Yun M. S. et al., 2011, MNRAS, preprint (arXiv:1109.6286)

This paper has been typeset from a TeX/LaTeX file prepared by the author.